Nonequilibrium dynamics of optical-lattice-loaded Bose-Einstein-condensate atoms: Beyond the Hartree-Fock-Bogoliubov approximation

Ana Maria Rey,[1,2] B. L. Hu,[1] Esteban Calzetta,[3] Albert Roura,[1] and Charles W. Clark[2]
[1]*Department of Physics, University of Maryland, College Park, Maryland 20742, USA*
[2]*Electron and Optical Physics Division, National Institute of Standards and Technology, Technology Administration, U. S. Department of Commerce, Gaithersburg, Maryland 20899-8410, USA*
[3]*Universidad de Buenos Aires—Ciudad Universitaria, 1428 Buenos Aires, Argentina*
(Received 13 October 2003; published 22 March 2004)

In this work a two-particle irreducible (2PI) closed-time-path (CTP) effective action is used to describe the nonequilibrium dynamics of a Bose-Einstein condensate selectively loaded into every third site of a one-dimensional optical lattice. The motivation of this work is the recent experimental realization of this system. Patterned loading methods may be useful for quantum computing with trapped atoms. This system also serves to illustrate many basic issues in nonequilibrium quantum-field theory pertaining to the dynamics of quantum correlations and fluctuations which goes beyond the capability of a mean-field theory. By numerically evolving in time the initial-state configuration using the Bose-Hubbard Hamiltonian an exact quantum solution is available for this system in the case of few atoms and wells. One can also use it to test various approximate methods. Under the 2PI CTP scheme with this initial configuration, three different approximations are considered: (a) the Hartree-Fock-Bogoliubov (HFB) approximation, (b) the next-to-leading-order $1/\mathcal{N}$ expansion of the 2PI effective action up to second order in the interaction strength, and (c) a second-order perturbative expansion in the interaction strength. We present detailed comparisons between these approximations and determine their range of validity by contrasting them with the exact many-body solution for a moderate number of atoms and wells. As a general feature we observe that because the second-order 2PI approximations include multiparticle scattering in a systematic way, they are able to capture damping effects exhibited in the exact solution, which a mean-field collisionless approach fails to produce. While the second-order approximations show a clear improvement over the HFB approximation, our numerical results show that they fail at late times, when interaction effects are significant.

DOI: 10.1103/PhysRevA.69.033610 PACS number(s): 03.75.Kk

I. DESCRIPTION OF THE PROBLEM

A Bose-Einstein condensate (BEC) loaded into an optical lattice provides an arena for the study of quantum coherence and fluctuation phenomena in many-body physics. Recent experiments have been able to achieve regimes where the standard mean-field description of a dilute interacting gas is inapplicable [1]. The description of the evolution of condensates far from equilibrium has also gained considerable importance in matter-wave physics, motivated by recent experimental realizations of colliding and collapsing condensates [2–4]. In this paper we investigate the dynamics of a Bose-Einstein condensate at zero temperature ($T=0$), which is initially loaded into every third site of a one-dimensional optical lattice. Such a system has recently been experimentally realized by the NIST group [5].

This system is not an eigenstate of the many-body Hamiltonian, and it thus evolves nontrivially in time. In the dilute gas limit, a mean-field approach is expected to give a good description of the condensate dynamics [6]. However, we show here that even in the case when the kinetic energy is comparable to the interaction energy, interatomic collisions play a crucial role in determining the quantum dynamics of the system, and therefore a mean-field collisionless approach is only accurate for short times. This result is demonstrated by comparison of the mean-field solution with exact numerical solutions of the tine-dependent Schrödinger equation for systems with small numbers of atoms ($N\sim 10$) and lattice sites ($I=2$ or 3).

Thus, in order to model the correct quantum dynamics of the system it is necessary to properly include scattering processes among particles. This task, however, is not easy for this particular system because contrary to the three-dimensional dilute gas case, where many-body effects introduce only a small change to the two-particle scattering properties in vacuum, the presence of the lattice and the low dimensionality of the system make the problem much less straightforward.

To date most theoretical descriptions of nonequilibrium dynamics of Bose-Einstein condensates (BECs) have been based on the time-dependent Gross-Pitaevskii equation coupled with extended kinetic theories that describe excitations in systems close to thermal equilibrium [7–9]. These approaches usually rely on the contact-interaction (or pseudopotential) approximation to pairwise atomic collisions, which is valid only at low collision energies. However, this approximation fails in the treatment of our system, so new methods are required. To treat far-from-equilibrium dynamics, we adopt a closed-time-path (CTP) [10] functional-integral formalism together with a two-particle irreducible (2PI) [11] effective action approach to derive the equations of motion. We retain terms of up to second order in the interaction strength when solving these equations. This method has been generalized for and applied to the establish-

ment of a quantum kinetic field theory [12–14] with applications to problems in gravitation and cosmology [15,16], particles and fields [17,18], BEC [19,20], and condensed-matter systems [21] as well as addressing the issues of thermalization and quantum phase transitions [22–24].

In Sec. II we present a brief review of the Bose-Hubbard model and its ground-state properties. In Sec. III we summarize the mean-field results obtained in previous studies [6]. In Sec. IV we introduce the 2PI generating functional to construct the 2PI effective action Γ_2 and Green's functions. In Sec. V we perform perturbative expansions on Γ_2 and define the various approximation schemes. In Sec. VI we introduce the CTP formalism. We then derive the equation of motion and discuss the results under each approximation scheme, starting with the Hartree-Fock-Bogoliubov (HFB) approximation in Sec. VII, followed by second-order expansions in Sec. VIII, which includes the $1/\mathcal{N}$ expansion and the full second-order expansion. The numerical implementation is discussed in Sec. IX. In Sec. X we present our results and determine the range of validity of the approximations by comparisons with the exact (numerical) solution. We conclude that our truncated 2PI approach is an effective tool for describing nonequilibrium dynamics in regimes in which higher-order correlations are unimportant. It includes effects of collisions that are not present in the HFB approximation, and goes beyond the Markovian assumptions generally used in kinetic theories.

II. BOSE-HUBBARD HAMILTONIAN

The dynamics of an ultracold bosonic gas in an optical lattice can be approximated by a Bose-Hubbard model where the system parameters are controlled by laser light. For a one-dimensional lattice the starting Hamiltonian is

$$\hat{H} = -J\sum_i (\hat{\Phi}_i^\dagger \hat{\Phi}_{i+1} + \hat{\Phi}_{i+1}^\dagger \hat{\Phi}_i) + \sum_i \epsilon_i \hat{\Phi}_i^\dagger \hat{\Phi}_i + \frac{1}{2} U \sum_i \hat{\Phi}_i^\dagger \hat{\Phi}_i^\dagger \hat{\Phi}_i \hat{\Phi}_i, \tag{1}$$

where $\hat{\Phi}_i$ and $\hat{\Phi}_i^\dagger$ are the bosonic operators that annihilate and create an atom on the site i. Here, the parameter U denotes the strength of the on-site repulsion of two atoms on the site i; the parameter ϵ_i denotes the energy offset of each lattice site due to an additional slowly varying external potential that might be present (such as a magnetic trap) and J denotes the hopping rate between adjacent sites. Because the next-to-nearest-neighbor amplitudes are typically two orders of magnitude smaller, tunneling to them can be neglected. The Bose-Hubbard Hamiltonian should be an appropriate model when the loading process produces atoms in the lowest vibrational state of each well, with a chemical potential smaller than the distance of the first vibrationally excited state. This is the case of the experiment that motivates this work [5].

Throughout this paper we denote the total number of atoms by N and the number of lattice sites by I. Here we consider only a one-dimensional homogeneous lattice with periodic boundary conditions. All results presented here are approximations to solving the problem of time evolution under the action of the Hamiltonian of Eq. (1). Treatment of the transverse degrees of freedom and harmonic confinement of atoms in the direction of the lattice are relegated to a future work.

The physics described by the Bose-Hubbard Hamiltonian is very rich and depends strongly on the parameters U, J, N, and I. Although the main focus of this paper is on treatment of a nonequilibrium system, it is useful to keep in mind the nature of the ground state for the different ranges of the physical parameters.

Ground-state properties

A detailed analysis of the superfluid properties of atoms in an optical lattice can be found in Ref. [25]. Here we only outline the principal ideas which can be important to understand the dynamical behavior discussed in this work.

A dimensionless parameter that is convenient to describe the different regimes of $\hat{H}$ is the coupling strength $\lambda \equiv NU/IJ$. Different from a homogeneous system without a lattice where at zero temperature the superfluid fraction is always unity, the presence of the lattice changes the superfluid properties and even at zero temperature, the superfluid fraction decreases with the lattice depth. For strong-coupling strengths [26] $\lambda > \lambda_{crit}$,

$$\lambda_{crit} \sim \frac{2N}{I^2}[2N + I + \sqrt{(2N+I)^2 + I^2}], \tag{2}$$

it is known that the ground state undergoes a quantum phase transition from a superfluid to a Mott insulator.

In the weakly interacting regime, $\lambda \ll 1$, where tunneling overwhelms the repulsion, to a good approximation quantum fluctuations can be neglected and the properties of the system can be described by replacing the operator on the lattice site i by a classical c number. It can be said that most of the atoms are in the zero quasimomentum state.

In the intermediate regime $1 < \lambda < \lambda_{crit}/2$ the interactions between the bosons can be very strong but the ground state is nevertheless a superfluid. For these interaction parameters a self-consistent HFB-Popov theory gives a good description of the system. However, different from the weak interacting regime where the depletion of the zero quasimomentum state is very small and has a little effect on the superfluid properties, in this intermediate regime, depleted atoms spread over the central part of the band and reduces the superfluid fraction. As interactions are further increased the depleted population completely fills the band and cancels the superfluid properties. The system reaches the Mott insulator regime, where atoms are completely localized at each lattice site, there is no coherence, and the eigenstates of the system are almost Fock states with a vanishing number fluctuations per lattice site.

The main purpose of this paper is to study the dynamics in the intermediate regime where the superfluid properties are important but quantum fluctuations cannot be ignored.

III. MEAN-FIELD DYNAMICS

By making the mean-field ansatz in the Bose-Hubbard Hamiltonian, that is, replacing the field operator by a c number $\phi_i(t)$, it is possible to show that the amplitudes $\phi_i(t)$ satisfy the discrete nonlinear Schrödinger equation (DNLSE) which in the case of zero external potential has the form

$$i\frac{\partial \phi_i}{\partial \tau} = -(\phi_{i-1} + \phi_{i+1}) + \frac{UN}{J}|\phi_i|^2\phi_i, \tag{3}$$

where we have defined a new time scaled $\tau \equiv tJ/\hbar$ and have imposed unit normalization upon ϕ having unit norm, so that N is the total number of atoms.

We treat a model case in which the initial occupancies of each third site are the same, and in which the condensate initially has a uniform phase. Thus at $\tau=0$, the amplitudes $\phi_i(\tau)$ are given by $\phi_{3i}(0)=\sqrt{3/I}$, $\phi_{3i+1}(0)=\phi_{3i+2}(0)=0$, where I is the total number of lattice sites. For an infinite lattice, or one with periodic boundary conditions, the amplitudes for all initially occupied sites ϕ_{3i} evolve identically in time, and the amplitudes for the initially unoccupied sites satisfy $\phi_{3i+1}(\tau)=\phi_{3i+2}(\tau)$ for all τ. This allows us to reduce the full set of equations (3) to a set of two coupled equations for $\phi_0(\tau)$ and $\phi_1(\tau)$.

The solutions $|\phi_0(\tau)|$ and $|\phi_1(\tau)|$ are oscillatory functions whose amplitudes and common period $T(\gamma)$ are determined by the parameter $\gamma \equiv 3(NU/IJ)=3\lambda$. It is useful to qualitatively divide the dynamical behavior into two regimes.

a. The tunneling dominated regime ($\gamma<1$). In this regime we find that the oscillation period is essentially constant, the role of interactions is relatively small, and the equations of motion are equivalent to those of a two-state Rabi problem. This system will undergo Rabi oscillations whereby atoms periodically tunnel from the initially occupied site into the two neighboring sites. For $\gamma=0$ the period of oscillation is $2\pi/3$.

b. Interaction dominated regime. The effect of interactions on the mean-field dynamics is to cause the energies of the initially occupied sites to shift relative to those of the unoccupied sites. As γ increases the tunneling between sites occurs at a higher frequency, but with reduced amplitude. The population of the initially occupied sites becomes effectively self-trapped by the purely repulsive pair interaction.

To check the validity of the mean-field approximation, we made comparisons with the exact many-body solution for six atoms and three wells. We use a modest number of atoms and lattice sites for the comparisons, due to the fact that the Hilbert space needed for the calculations increases rapidly with the number of atoms and wells. The exact solution was obtained by evolving an initial state $(e^{-N/2}e^{\sqrt{N}\hat{\Phi}_o^\dagger}|0\rangle)\otimes|0\rangle \otimes|0\rangle$ with the Bose-Hubbard Hamiltonian. The initial state represents just a coherent state with an average of N atoms in the initial populated well. (See Sec. IX A.)

In Fig. 1 we plot the average population per well $\langle\hat{\Phi}_i^\dagger(t)\hat{\Phi}_i(t)\rangle$ and the condensate population per well $|\langle\hat{\Phi}_i(t)\rangle|^2$ and compare them with the mean-field predictions, i.e., $|\phi_i(t)|^2$, for three different values of γ. The salient features observed in these comparisons are as follows.

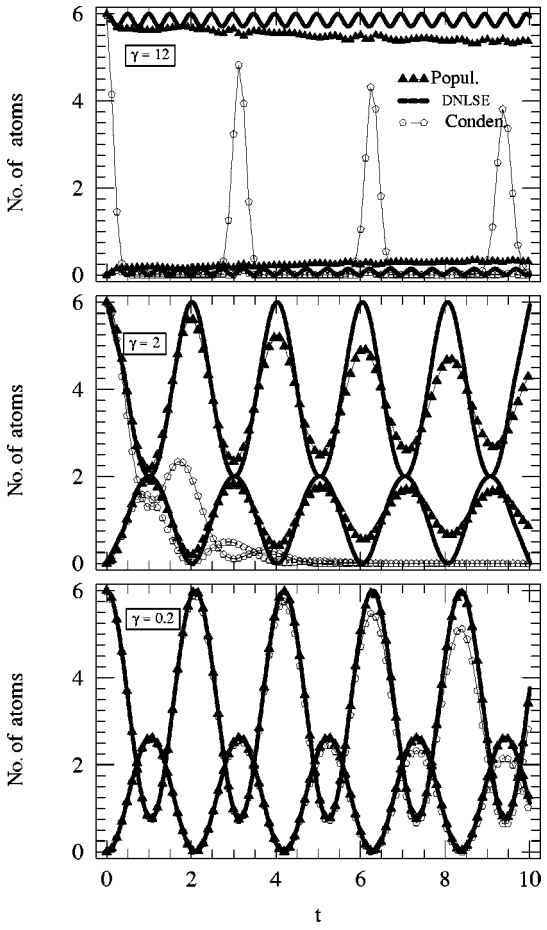

FIG. 1. Comparisons between the exact and the DNLSE solutions for six atoms and three wells. The time is given in units of $\hbar/J$. Top panel, strongly correlated regime ($\gamma=12$); middle panel, intermediate regime ($\gamma=2$); bottom panel, weakly interacting regime ($\gamma=0.2$). The solid line is the DNLSE prediction for the population per well: $|\phi_0(t)|^2$ and $|\phi_{1,2}(t)|^2$ [see Eq. (3)], the triangles are used to represent the exact solution for the population per well calculated using the Bose-Hubbard Hamiltonian [Eq. (1)]: $\langle\hat{\Phi}_0^\dagger\hat{\Phi}_0\rangle, \langle\hat{\Phi}_{1,2}^\dagger\hat{\Phi}_{1,2}\rangle$. The pentagons show the condensate population per well calculated from the exact solution: $|\langle\hat{\Phi}_0\rangle|^2$ and $|\langle\hat{\Phi}_{1,2}\rangle|^2$. Due to the symmetry of the initial periodic conditions the curves for the $i=1$ and 2 wells are the same in all depicted curves.

(1) Weakly interacting regime ($\gamma=0.2$): In this regime the DNLSE gives a good description of the early time dynamics. We observe in Fig. 1 that the total population per well predicted by the mean-field solution agrees with the exact solution and also that the condensate population remains big for the time under consideration. We expect the semiclassical approach to be valid for time scales less than the inverse energy-level spacing. In Ref. [27] the authors show for two lattice sites the validity of the semiclassical approach when $t<t_{cl}\sim N/I\gamma$. This time scale is in good agreement with the numerical results shown in Fig. 1. After t_{cl} quantum effects become important.

(2) Intermediate regime ($\gamma=2$): Quantum fluctuations lead to a nontrivial modulation of the classical oscillations. In this regime the ratio between interaction and kinetic energy is small enough to allow the atoms to tunnel but not too small

to make interaction effects negligible. Mean-field results are accurate only for a short time. In this regime, the exact solution exhibits damped oscillations of the atomic population. Quantum scattering effects are crucial, even for rather early times.

To understand the dynamics in the weak and intermediate regimes, we have to focus on the coherent properties of the system. Even though interactions can be strong, the ground state is indeed superfluid. If we look at the initial coherence of the system, determined by $\langle\hat{\Phi}_i^\dagger(0)\hat{\Phi}_j(0)\rangle_{i\neq j}$, it can be seen that it is zero due to the patterned loading. However, this is no longer the case for $t>0$, and nonzero correlations are developed in the dynamics. The dynamical restoration of the phase coherence which tends to distribute atoms uniformly among the lattice sites and to damp the oscillations characterizes the dynamics in the superfluid regime. In Ref. [27], the authors show, not for a patterned loaded initial state but for an initial Mott state also with zero initial phase coherence, how the phase coherence is restored dynamically.

(3) Strongly correlated regime ($\gamma=12$): The system exhibits macroscopic quantum self-trapping of the population. Qualitatively, both the mean field and the exact solutions agree, in the sense that both predict self-trapping of atoms in the initially populated wells, due to interactions. However, the fast decrease of the condensate population and its subsequent revivals (as found in the exact solutions) give us an idea of the importance of correlation effects beyond mean field. The collapse and revivals of the condensate in this strong interacting regime and the importance of quantum effects have been experimentally observed [28].

Even though there is not initial coherence between adjacent sites due to the patterned loading procedure we are still preparing the system in a superfluid state in the initial populated well. At time $t=0$ we have a condensate fraction of order one. However, the ground state of the system is not superfluid. It is expected then that, after some time, the phase is going to randomize and this will lead to the collapse of the condensate population. After the collapse, the system will remain for a while with zero condensate population. However, it cannot remain zero forever because we are dealing with a close quantum system, with finite recurrence time. Therefore at some time t_{rev} we expect the condensate to revive again. The collapses and revivals of the condensate population in the strong interacting regime can be easily estimated by considering the energy spectrum. In this regime the energy eigenstates of the system are almost number Fock states and the energy spectrum is almost quadratic, $E_n \approx n(n-1)U/2$. The dynamics of the system is described by the interference of the different n-particle Fock states that span the coherent state of the initially populated well. At integer values of $t_{rev}=(U/h)^{-1}$, the phase factors add to an integer value of 2π, leading to a revival of the initial state. This time scale agrees with the one estimated in Ref. [29] for a more general situation. In this reference, they also show how the collapse time t_{coll} depends on the variance of the initial atomic distribution and is given by $t_{coll}\sim t_{rev}/(2\pi\sigma)$. If the initial state is a coherent state, the initial distribution is Poissonian and t_{coll} is given by $t_{coll}\sim\hbar/(\sqrt{N}U)$. For the parameters used in the strong correlated regime, $\gamma=12$ and $N=6$, we observe that the estimated collapses and revival times are in agreement with what is shown in Fig. 1.

Because our main interest is the tunneling dynamics we will focus on the intermediate regime, where the ratio U/J is small but interaction effects are not negligible. In this regime a perturbative expansion around U/J still makes sense.

IV. 2PI EFFECTIVE ACTION $\Gamma(\phi,G)$

The first requirement for the study of nonequilibrium processes is a general initial-value formulation depicting the dynamics of interacting quantum fields. The CTP or Schwinger-Keldysh effective action formalism [10] serves this purpose. The second requirement is to describe the evolution of the correlation functions and the mean field on an equal footing. The 2PI formalism [11] where the correlation functions appear also as independent variables serves this purpose. By requiring the generalized (master) CTP effective action [13] to be stationary with respect to variations of the correlation functions an infinite set of coupled (Schwinger-Dyson) equations for the correlation functions is obtained which is a quantum analog of the Bogoliubov-Born-Green-Kirkwood-Yvon hierarchy. The 2PI effective action produces two such functions in this hierarchy. In this section we shall focus on the 2PI formalism and then upgrade it to the CTP version in the following section.

The classical action associated with the Bose-Hubbard Hamiltonian (1), is given in terms of the complex fields Φ_i and Φ_i^* by

$$S[\Phi_i^*,\Phi_i]=\int dt\sum_i i\hbar\Phi_i^*(t)\partial_t\Phi_i(t)+\int dt\sum_i J[\Phi_i^*(t)\Phi_{i+1}(t)+\Phi_i(t)\Phi_{i+1}^*(t)]-\int dt\sum_i\frac{U}{2}\Phi_i^*(t)\Phi_i^*(t)\Phi_i(t)\Phi_i(t). \tag{4}$$

To compactify our notation we introduce $\Phi_i^a(a=1,2)$ defined by

$$\Phi_i=\Phi_i^1,\quad \Phi_i^*=\Phi_i^2. \tag{5}$$

In terms of these fields the classical action takes the form

$$S[\Phi]=\int dt\sum_i\frac{1}{2}h_{ab}\Phi_i^a(t)\hbar\partial_t\Phi_i^b(t)+\int dt\sum_i\left(J\sigma_{ab}\Phi_{i+1}^a(t)\Phi_i^b(t)-\frac{U}{4\mathcal{N}}[\sigma_{ab}\Phi_i^a(t)\Phi_i^b(t)]^2\right), \tag{6}$$

where $\mathcal{N}$ is the number of fields,which is 2 in this case, and summation over repeated field indices $a,b=(1,2)$ is implied. h_{ab} and σ_{ab} are matrices defined as

$$h_{ab} = i\begin{pmatrix} 0 & -1 \\ 1 & 0 \end{pmatrix}, \quad \sigma_{ab} = \begin{pmatrix} 0 & 1 \\ 1 & 0 \end{pmatrix}. \tag{7}$$

In terms of the familiar Pauli matrices, $\sigma_{ab}=\sigma_x$ and $h_{ab}=-\sigma_y$.

After second quantization the fields Φ_i^a are promoted to operators. We denote the expectation value of the field operator or mean field by $\phi_i^a(t)$ and the expectation value of the composite field by $G_{ij}^{ab}(t,t')$. Physically, $|\phi_i^a(t)|^2$ is the condensate population and the composite fields determine the fluctuations around the mean field:

$$\phi_i^a(t) = \langle \Phi_i^a(t) \rangle, \tag{8}$$

$$G_{ij}^{ab}(t,t') = \langle T_C \Phi_i^a(t) \Phi_i^b(t') \rangle - \langle \Phi_i^a(t) \rangle \langle \Phi_i^b(t') \rangle. \tag{9}$$

The brackets denote taking the expectation value with respect to the density matrix and T_C denotes time ordering along a contour C in the complex plane.

All correlation functions of the quantum theory can be obtained from the effective action $\Gamma[\phi,G]$, the two-particle irreducible generating functional for Green's functions parametrized by $\phi_i^a(t)$ and the composite field $G_{ij}^{ab}(t,t')$. To get an expression for the effective action we first define the functional $Z[\mathbf{J},\mathbf{K}]$ [11] as

$$\begin{aligned} Z[\mathbf{J},\mathbf{K}] &= e^{i/\hbar W[\mathbf{J},\mathbf{K}]} \\ &= \prod_a \int D\Phi^a \exp\left\{ \frac{i}{\hbar} \left(S[\Phi] + \int dt \sum_i \mathbf{J}_{ia}(t) \Phi_i^a(t) \right.\right. \\ &\quad \left.\left. + \frac{1}{2} \int dt dt' \sum_{ij} \Phi_i^a(t) \Phi_j^b(t') \mathbf{K}_{ijab}(t,t') \right) \right\}, \end{aligned} \tag{10}$$

where we have introduced the following index lowering convention:

$$X_a = \sigma_{ab} X^b. \tag{11}$$

The functional integral (10) is a sum over classical histories of the field Φ_i^a in the presence of the local source $\mathbf{J}_{ia}$ and the nonlocal source $\mathbf{K}_{ijab}$. The coherent-state measure is included in $D\Phi$. The addition of the two-particle source term is what characterizes the 2PI formalism.

We define $\Gamma[\phi,G]$ as the double Legendre transform of $W[\mathbf{J},\mathbf{K}]$ such that

$$\frac{\delta W[\mathbf{J},\mathbf{K}]}{\delta \mathbf{J}_{ia}(t)} = \phi_i^a(t), \tag{12}$$

$$\frac{\delta W[\mathbf{J},\mathbf{K}]}{\delta \mathbf{K}_{ijab}(t,t')} = \frac{1}{2}[\phi_i^a(t)\phi_i^b(t') + G_{ij}^{ab}(t,t')]. \tag{13}$$

Expressing $\mathbf{J}$ and $\mathbf{K}$ in terms of ϕ and G yields

$$\begin{aligned} \Gamma[\phi,G] &= W[\mathbf{J},\mathbf{K}] - \int dt \sum_i \mathbf{J}_{ia}(t) \phi_i^a(t) \\ &\quad - \frac{1}{2} \int dt dt' \sum_{ij} \phi_i^a(t) \phi_j^b(t') \mathbf{K}_{ijab}(t,t') \\ &\quad - \frac{1}{2} \int dt dt' \sum_{ij} G_{ij}^{ab}(t,t') \mathbf{K}_{ijab}(t,t'). \end{aligned} \tag{14}$$

From this equation the following identity can be derived:

$$\frac{\delta \Gamma[\phi,G]}{\delta \phi_i^a(t)} = -\mathbf{J}_{ia}(t) - \int dt' \sum_j [\mathbf{K}_{ijad}(t,t')] \phi_j^d(t'), \tag{15}$$

$$\frac{\delta \Gamma[\phi,G]}{\delta G_{ij}^{ab}(t,t')} = -\frac{1}{2} \mathbf{K}_{ijab}(t,t'). \tag{16}$$

In order to get an expression for $\Gamma[\phi,G]$ notice that by using Eq. (10) for $W[\mathbf{J},\mathbf{K}]$ and placing it in Eq. (15) for $\Gamma[\phi,G]$, it can be written as

$$\begin{aligned} \exp\left(\frac{i}{\hbar}\Gamma[\phi,G]\right) &= \prod_a \int D\Phi^a \exp\left\{ \frac{i}{\hbar} \left(S[\Phi] + \int dt_i \mathbf{J}_{ia}(t) [\Phi_i^a(t) - \phi_i^a(t)] \right.\right. \\ &\quad \left.\left. + \frac{1}{2} \int dt_i dt_j' [\Phi_i^a(t) \mathbf{K}_{ijab}(t,t') \Phi_j^b(t') - \phi_i^a(t) \mathbf{K}_{ijab}(t,t') \phi_j^b(t')] - \frac{1}{2} \mathrm{Tr} G \mathbf{K} \right) \right\} \\ &= \prod_a \int D\Phi^a \exp\left\{ \frac{i}{\hbar} \left(S[\Phi] - \int dt_i \frac{\delta \Gamma[\phi,G]}{\delta \phi_i^a(t)} [\Phi_i^a(t) - \phi_i^a(t)] - \int dt_i dt_j' [\Phi_i^a(t) - \phi_i^a(t)] \frac{\delta \Gamma[\phi,G]}{\delta G_{ij}^{ab}(t,t')} \right.\right. \\ &\quad \left.\left. \times [\Phi_i^b(t') - \phi_i^b(t')] + \mathrm{Tr} G \frac{\delta \Gamma[\phi,G]}{\delta G} \right) \right\}, \end{aligned} \tag{17}$$

where Tr means taking the trace. For simplicity we have denoted $\int dt \Sigma_i$ by $\int dt_i$. Defining the fluctuation field, $\varphi_i^a \equiv \Phi_i^a - \phi_i^a$, we have

$$\Gamma[\phi,G] - \mathrm{Tr}\, G\frac{\delta\Gamma[\phi,G]}{\delta G} = -i\hbar \ln\prod_a \int D\varphi^a \exp\left(\frac{i}{\hbar}S[\phi,G;\varphi]\right), \quad (18)$$

$$S[\phi,G;\varphi] = S[\phi+\varphi] - \int dt_i \frac{\delta\Gamma[\phi,G]}{\delta\phi_i^a(t)}\varphi_i^a(t) - \int dt_i dt_j' \varphi_i^a(t)\frac{\delta\Gamma[\phi,G]}{\delta G_{ij}^{ab}(t,t')}\varphi_i^b(t'). \quad (19)$$

By introducing the classical inverse propagator $iD^{-1}(\phi)$ given by

$$iD_{ijab}(t,t')^{-1} = \frac{\delta S[\phi]}{\delta\phi_i^a(t)\delta\phi_j^b(t')} = [\delta_{ij}h_{ab}\partial_t + J(\delta_{i+1j}+\delta_{i-1j})\sigma_{ab}]\delta(t-t') - \frac{U}{\mathcal{N}}[2\phi_{ia}(t)\phi_{ib}(t) + \sigma_{ab}\phi_i^c(t)\phi_{ic}(t)]\delta_{ij}\delta(t-t'), \quad (20)$$

the solution of the functional integro-differential equation (18) can be expressed as

$$\Gamma[\phi,G] = S[\phi] + \frac{i}{2}\mathrm{Tr}\,\ln G^{-1} + \frac{i}{2}\mathrm{Tr}\, D^{-1}(\phi)G + \Gamma_2[\phi,G] + \text{const.} \quad (21)$$

The quantity $\Gamma_2[\phi,G]$ is conveniently described in terms of the diagrams generated by the interaction terms in $S[\phi+\varphi]$ which are of cubic and higher orders in φ:

$$S_{int}[\phi+\varphi] = -\frac{U}{4\mathcal{N}}\int dt_i[\varphi_{ib}(t)\varphi_i^b(t)]^2 - \frac{U}{\mathcal{N}}\int dt_i \varphi_i^a(t)\phi_{ia}(t)\varphi_i^b(t)\varphi_{ib}(t). \quad (22)$$

It consists of all two-particle irreducible vacuum graphs (the diagrams representing these interactions do not become disconnected by cutting two propagator lines) in the theory with propagators set equal to G and vertices determined by the interaction terms in $S[\phi+\varphi]$.

Since physical processes correspond to vanishing sources **J** and **K**, the dynamical equations of motion for the mean field and the propagators are found by using the expression (21) in Eqs. (15) and (16), and setting the right-hand side equal to zero. This procedure leads to the following equations:

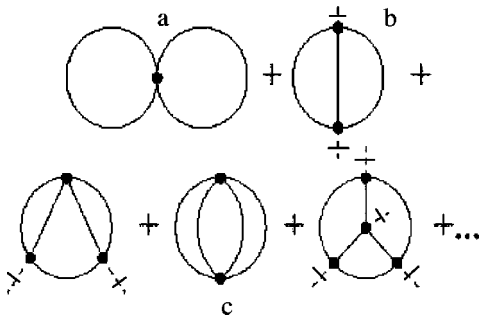

FIG. 2. Two-loop (upper row) and three-loop diagrams (lower row) contributing to the effective action. Explicitly, the diagram (a) is what we call the *double-bubble*, (b) the *setting sun*, and (c) the *basketball*.

$$h_{ab}\hbar\partial_t\phi_i^b(t) = -J[\phi_{i+1a}(t)+\phi_{i-1a}(t)] + \frac{U}{\mathcal{N}}[\phi_{id}(t)\phi_i^d(t) + G_{iic}^c(t,t)]\phi_{ia}(t) + \frac{U}{\mathcal{N}}\left[(G_{iiad}(t,t)+G_{iida}(t,t)]\phi_i^d(t) - \frac{\delta\Gamma_2[\phi,G]}{\delta\phi_i^a(t)}\right. \quad (23)$$

and

$$G_{ijab}^{-1}(t,t') = D_{ijab}(t,t')^{-1} - \Sigma_{ijab}(t,t'), \quad (24)$$

$$\Sigma_{ijab}(t,t') \equiv 2i\frac{\delta\Gamma_2[\phi,G]}{\delta G_{ij}^{ab}(t,t')}. \quad (25)$$

Equation (24) can be rewritten as a partial differential equation suitable for initial-value problems by convolution with G. This differential equation reads explicitly

$$h_c^a\hbar\partial_t G_{ij}^{cb}(t,t') = -J[G_{i+1j}^{ab}(t,t') + G_{i-1j}^{ab}(t,t')] + \frac{U}{\mathcal{N}}[\phi_{id}(t)\phi_i^d(t)]G_{ij}^{ab}(t,t') + \frac{2U}{\mathcal{N}}\phi_i^a(t)G_{ij}^{cb}(t,t')\phi_{ic}(t) + i\int dt_k''\Sigma_{ikc}^a(t,t'')G_{kj}^{cb}(t'',t') + i\delta^{ab}\delta_{ij}\delta(t-t'). \quad (26)$$

The evolution of ϕ^a and G^{ab} is determined by Eqs. (24) and (26) once $\Gamma_2[\phi,G]$ is specified.

V. PERTURBATIVE EXPANSION OF $\Gamma_2(\phi,G)$ AND APPROXIMATION SCHEMES

The diagrammatic expansion of Γ_2 is illustrated in Fig. 2, where two- and three-loop vacuum diagrams are shown. The dots where four lines meet represent interaction vertices. The expression corresponding to each vacuum diagram should be multiplied by a factor $(-i)^l(i)^{s-2}$, where l is the number of solid lines and s the number of loops the diagram contains.

The action Γ including the full diagrammatic series for Γ_2 gives the full dynamics. It is of course not feasible to obtain an exact expression for Γ_2 in a closed form. Various approximations for the full 2PI effective action can be obtained by truncating the diagrammatic expansion for Γ_2. Which approximation is most appropriate depends on the physical problem under consideration.

A. The standard approaches

(1) Mean-field approximation: If, in Eq. (21), we discard all terms to the right of $S[\phi]$, we recover the DNLSE of Eq. (3). This gives us the usual mean-field description, in which the system remains a pure condensate.

(2) Bogoliubov (one-loop) approximation: The next approximation consists of discarding Γ_2 altogether. This yields the so-called Bogoliubov or one-loop approximation whose limitations have been extensively documented in the literature [30,31].

(3) Time-dependent HFB approximation: A truncation of Γ_2 retaining only the first-order diagram in U, i.e., keeping only the *double-bubble* diagram, Fig. 2(a), yields equations of motion of ϕ and G which correspond to the time-dependent HFB approximation. This approximation violates Goldstone's theorem, but conserves energy and particle number [7,32,33]). The HFB equations can also be obtained by using cumulant expansions up to the second order [34] in which all cumulants containing three or four field operators are neglected. The HFB approximation neglects multiple scattering. It can be interpreted as an expansion in terms of Ut/J (where t is the time of evolution) and is good for the description of short-time dynamics or weak interaction strengths. It will be described in Sec. VII.

B. Higher-order expansions

We make a few remarks on the general properties of higher-order expansions and then specialize to two approximations.

a. 2PI and ladder diagrams. Since the work of Beliaev [35] and Popov [36] it is well known in the literature (see, for example, Refs. [19,37]) that including higher-order terms in a diagrammatic expansion corresponds to renormalizing the bare interaction potential to the four-point vertex, thus accounting for the repeated scattering of the bosons. In Ref. [38] the authors have shown explicitly for a homogeneous Bose gas that taking into account the two-loop contribution to the 2PI effective action leads to diagrams topologically identical to those found by Beliaev but with the exact propagator instead of the one-loop propagator. In the dilute gas limit, where the interparticle distance is large compared with the s-wave scattering length, the ladder diagrams give the largest contribution to the four-point vertex. Every rung in a ladder contributes to a factor proportional to Um. **(**In the presence of the lattice m should be replaced by the effective mass $m^*[m^* \sim \hbar^2/(Ja^2)]$ with a as the lattice spacing.**)** The ladder resummation results in an effective potential which is called the T matrix. To lowest order in the diluteness parameter, the T matrix in three-dimensional systems can be approximated by a constant proportional to the scattering length (pseudopotential approximation). However this approximation is only valid in the weak interaction limit and neglects all momentum dependence which appear in the problem as higher-order terms. In that sense the 2PI effective action approach allows us to go beyond the weakly interacting limit in a systematic way and to treat collisions more accurately.

b. Nonlocal dissipation and non-Markovian dynamics. Higher-order terms lead to nonlocal equations and dissipation. The presence of nonlocal terms in the equations of motion is a consequence of the fact that the 2PI effective action really corresponds to a further approximation of the master effective equation [13]. The 2PI effective action is obtained by the *slaving* of the three-point function C_3 to the mean field and G with a particular choice of boundary conditions. See Ref. [13] for further details.

Non-Markovian dynamics is a generic feature of the nPI formalism which yields integro-differential equations of motion. This makes numerical solution difficult, but is a necessary price to pay for a fuller account of the quantum dynamics. Many well acknowledged approaches to the quantum kinetics of such systems adopt either explicitly or implicitly (or at the end what amounts to) a Markovian approximation [39]. It assumes that only the current configuration of the system, but not its history, determines its future evolution. Markovian approximations are made if one assumes instantaneous interactions, or in the kinetic theory context that the time scales between the duration of binary collisions τ_0 and the inverse collision rate τ_c are well separated. In the low kinetic energy, weak interacting regime the time between collisions (or mean free path) is long compared to the reaction time (or scattering length): $\tau_c \gg \tau_0$. The long separation between collisions and the presence of intermediate weak fluctuations allow for a rapid decay of the temporal and spatial correlations created between collision partners, which one can use to justify the Markovian approximation. However, in the problem at hand, owing to the presence of the lattice which confines the atoms to the bottom of the wells with enhanced interaction effects, the low dimensionality of the system, and the far-from-equilibrium initial conditions, non-Markovian dynamics needs to be confronted squarely. That is, the rationale for our adoption of the CTP 2PI scheme. Now, for the specifics, we describe the following.

(1) Second-order expansion: A truncation retaining diagrams of second order in U consists of the *double-bubble*, the *setting-sun*, and the *basketball* (see Fig. 2). By including the setting-sun and the basketball in the approximations we are taking into account two particle scattering processes [14,16]. Second order terms lead to integro- differential equations which depend on the time history of the system.

(2) Large-$\mathcal{N}$ approximation: The $1/\mathcal{N}$ expansion is a controlled nonperturbative approximation scheme which can be used to study nonequilibrium quantum-field dynamics in the regime of strong interactions [22,23]. In the large $\mathcal{N}$ approach the field is modeled by $\mathcal{N}$ fields and the quantum-field generating functional is expanded in powers of $1/\mathcal{N}$. In this sense the method is a controlled expansion in a small parameter but unlike perturbation theory in the coupling constant, which corresponds to an expansion around the vacuum, the large $\mathcal{N}$ expansion corresponds to an expansion

of the theory about a strong quasiclassical field.

In this work we derive the equations of motion and perform numerical calculations up to the second order in the coupling constant U. This will enable us to determine the range of validity of three types of approximations described above, namely, (a) the HFB, (b) the full second order, and (c) the next-to-leading-order (NLO) large $\mathcal{N}$ expansion up to second order in U (in the figures we use the shorthand HFB, 2nd, and $1/\mathcal{N}$, respectively) by comparison with the exact many body solution for a moderate number of atoms and wells.

VI. CTP FORMALISM

In order to describe the nonequilibrium dynamics we will now specify the contour of integration in Eqs. (24) and (26) to be the Schwinger-Keldysh contour [10] along the real-time axis or CTP contour. The Schwinger-Keldysh formalism is a powerful method for deriving real and causal evolution equations for the expectation values of quantum operators for nonequilibrium fields. The basic idea of the CTP formalism relies on the fact that a diagonal matrix element of a system at a given time $t=0$ can be expressed as a product of transition matrix elements from $t=0$ to t' and the time-reverse (complex conjugate) matrix element from t' to 0 by inserting a complete set of states into this matrix element at the later time t'. Since each term in the product is a transition matrix element of the usual or time-reversed kind, the standard path-integral representation for each one can be introduced. However, to get the generating functional we seek, we have to require that the forward time evolution takes place in the presence of a source J^+ but the reversed time evolution takes place in the presence of a different source J^-, otherwise all the dependence on the source drops out.

The doubling of sources, the fields, and integration contours suggest introducing a 2×2 matrix notation. This notation has been discussed extensively in the literature (see Refs. [12,14]). However we are going to follow Refs. [22,23] and introduce the CTP formalism in our equation of motion by using the composition rule for transition amplitudes along the time contour in the complex plane. This way is cleaner notationally and has the advantage that all the functional formalism of the preceding section may be taken with the only difference of path ordering according to the complex time contour C_{CTP} in the time integrations.

The two-point functions are decomposed as

$$G_{ij}^{ab}(t,t') = \theta_{ctp}(t,t')G_{ij}^{ab>}(t,t') + \theta_{ctp}(t,t')G_{ij}^{ab<}(t,t'), \tag{27}$$

where

$$G_{ij}^{ab>}(t,t') = \langle \varphi_i^a(t)\varphi_j^b(t')\rangle, \tag{28}$$

$$G_{ij}^{ab<}(t,t') = \langle \varphi_i^b(t')\varphi_j^a(t)\rangle, \tag{29}$$

with φ_i being the fluctuation field defined prior Eq. (17) and $\theta_{\mathrm{CTP}}(t-t')$ being the CTP complex contour ordered theta function defined by

$$\theta_{\mathrm{CTP}}(t,t') = \begin{cases} \theta(t,t') & \text{for } t \text{ and } t' \text{ both on } C^+ \\ \theta(t,t') & \text{for } t \text{ and } t' \text{ both on } C^- \\ 1 \text{ for } t \text{ on } C^- \text{ and } t' \text{ on } C^+ \\ 0 \text{ for } t \text{ on } C^+ \text{ and } t' \text{ on } C^-. \end{cases} \tag{30}$$

With these definitions the matrix indices are not required. When integrating over the second half C^-, we have to multiply by a negative sign to take into account the opposite direction of integration.

To show explicitly that the prescription for the CTP integration explained above does lead to a well-posed initial-value problem with causal equations, let us explicitly consider the integral in Eq. (26). The integrand has the CTP ordered form

$$\begin{aligned} \Sigma(t,t'')G(t'',t') = {} & \theta_{\mathrm{CTP}}(t,t'')\theta_{\mathrm{CTP}}(t'',t')\Sigma^{>}(t,t'')G^{>}(t'',t') \\ & + \theta_{\mathrm{CTP}}(t,t'')\theta_{\mathrm{CTP}}(t',t'')\Sigma^{>}(t,t'')G^{<}(t'',t') \\ & \times \theta_{\mathrm{CTP}}(t'',t)\theta_{\mathrm{CTP}}(t'',t')\Sigma^{<}(t,t'')G^{>}(t'',t') \\ & + \theta_{\mathrm{CTP}}(t'',t)\theta_{\mathrm{CTP}}(t',t'')\Sigma^{<}(t,t'')G^{<}(t'',t'), \end{aligned} \tag{31}$$

where we have omitted the indices because they are not relevant for the discussion. Using the rule for CTP contour integration we get

$$\begin{aligned} \int dt''\Sigma(t,t'')G(t'',t') = {} & \int_0^t dt''[\theta(t'',t')\Sigma^{>}(t,t'')G^{>}(t'',t') \\ & + \theta(t'',t'')\Sigma^{>}(t,t')G^{<}(t'',t')] \\ & + \int_t^\infty dt''[\theta(t'',t')\Sigma^{<}(t,t'')G^{>}(t'',t') \\ & + \theta(t',t'')\Sigma^{<}(t,t'')G^{<}(t'',t')] \\ & - \int_0^\infty dt''\Sigma^{<}(t,t'')G^{>}(t'',t'). \end{aligned} \tag{32}$$

If $t>t'$, we have

$$\begin{aligned} \int dt''\Sigma(t,t'')G(t'',t') = {} & \int_0^t dt''[\Sigma^{>}(t,t'') - \Sigma^{<}(t,t'')]G^{>}(t'',t') \\ & - \int_0^{t'} dt''\Sigma^{>}(t,t'') \\ & \times [G^{>}(t'',t') - G^{<}(t'',t')]. \end{aligned} \tag{33}$$

On the other hand, if $t<t'$,

$$\begin{aligned} \int dt''\Sigma(t,t'')G(t'',t') = {} & \int_0^t dt''[\Sigma^{>}(t,t'') - \Sigma^{<}(t,t'')]G^{<}(t'',t') \\ & - \int_0^{t'} dt''\Sigma^{>}(t,t'') \\ & \times [G^{>}(t'',t') - G^{<}(t'',t')]. \end{aligned} \tag{34}$$

The above equations are explicitly causal.

It is convenient to express the evolution equations in terms of two independent two-point functions which can be associated to the expectation values of the commutator and the anticommutator of the fields. We define, following Ref. [23], the functions

$$G_{ij}^{(F)ab}(t,t') = \frac{1}{2}[G_{ij}^{ab>}(t,t') + G_{ij}^{ab<}(t,t')], \tag{35}$$

$$G_{ij}^{(\rho)ab}(t,t') = i[G_{ij}^{ab>}(t,t') - G_{ij}^{ab<}(t,t')], \tag{36}$$

where the (F) functions are usually called statistical propagators and the (ρ) spectral functions. (See Ref. [40].) With these definitions Eq. (26) can be rewritten as

$$\begin{aligned} h_c^a \hbar \partial_t G_{ij}^{(F)cb}(t,t') = &- J[G_{i+1j}^{(F)ab}(t,t') + G_{i-1j}^{(F)ab}(t,t')] \\ &+ \frac{U}{\mathcal{N}}[\phi_{ic}(t)\phi_i^c(t)G_{ij}^{(F)ab}(t,t')] \\ &+ \frac{2U}{\mathcal{N}}[\phi_i^a(t)G_{ij}^{(F)cb}(t,t')\phi_{ic}(t)] \\ &+ \int_0^t dt_k'' \sum_{ik}^{(\rho)ac}(t,t'')G_{kj\ c}^{(F)\ b}(t'',t') \\ &- \int_0^{t'} dt_k'' \sum_{ik}^{(F)ac}(t,t'')G_{kjc}^{(\rho)b}(t'',t'), \end{aligned} \tag{37}$$

$$\begin{aligned} h_c^a \hbar \partial_t G_{ij}^{(\rho)cb}(t,t') = &- J[G_{i+1j}^{(\rho)ab}(t,t') + G_{i-1j}^{(\rho)ab}(t,t')] \\ &+ \frac{U}{\mathcal{N}}[\phi_{ic}(t)\phi_i^c(t)G_{ij}^{(\rho)ab}(t,t')] \\ &+ \frac{2U}{\mathcal{N}}[\phi_i^a(t)G_{ij}^{(\rho)cb}(t,t')\phi_{ic}(t)] \\ &+ \int_{t'}^t dt_k'' \Sigma_{ik}^{(\rho)ac}(t,t'')G_{kjc}^{(\rho)b}(t'',t'). \end{aligned} \tag{38}$$

In particular, we define the normal, ρ, and anomalous, m, spectral and statistical functions as

$$G_{ij}^{21(F)}(t,t') \equiv \rho_{ij}^{(F)}(t,t') = \frac{1}{2}\langle \varphi_i^\dagger(t)\varphi_j(t') + \varphi_j(t')\varphi_i^\dagger(t)\rangle, \tag{39}$$

$$G_{ij}^{21(\rho)}(t,t') \equiv \rho_{ij}^{(\rho)}(t,t') = i\langle \varphi_i^\dagger(t)\varphi_j(t') - \varphi_j(t')\varphi_i^\dagger(t)\rangle, \tag{40}$$

$$G_{ij}^{11(F)}(t,t') \equiv m_{ij}^{(F)}(t,t') = \frac{1}{2}\langle \varphi_i(t)\varphi_j(t') + \varphi_j(t')\varphi_i(t)\rangle, \tag{41}$$

$$G_{ij}^{11(\rho)}(t,t') \equiv m_{ij}^{(\rho)}(t,t') = i\langle \varphi_i(t)\varphi_j(t') - \varphi_j(t')\varphi_i(t)\rangle. \tag{42}$$

With these relations in place, we now proceed to derive the time-evolution equations for the mean field and the two-point functions from the CTP 2PI effective action for the Bose-Hubbard model under the three approximations described before.

VII. HFB APPROXIMATION

As remarked in Sec. II the first-order mean-field approximation leads to a DNLSE which includes only the contribution from the condensate. The HFB equations go beyond the first-order approximation and include the leading-order contribution of Γ_2. They describe the coupled dynamics of condensate and noncondensate atoms which arise from the most important scattering processes which are direct, exchange, and pair excitations. The basic damping mechanisms present in the HFB approximation are Landau and Beliaev damping associated with the decay of an elementary excitation into a pair of excitations in the presence of condensate atoms, Refs. [33,41]. However, these kinds of damping [42] found in the HFB approximation (due to phase mixing, as in the Vlasov equation Ref. [43]) are different in nature from the collisional dissipation (as in the Boltzmann equation) responsible for thermalization processes. Multiple-scattering processes are neglected in this approximation. We expect the HFB equations to give a good description of the dynamics in the collisionless regime when interparticle collisions play a minor role.

The leading-order contribution of Γ_2 is represented by the double-bubble diagram. Its contribution to Γ_2 is ϕ independent and has an analytic expression of the form

$$\Gamma_2^{(1)}[G] = -\frac{U}{4\mathcal{N}}\int dt_i[G_{iia}^a(t,t)G_{iib}^b(t,t) + 2G_{iiab}(t,t)G_{ii}^{ab}(t,t)], \tag{43}$$

the factor of 2 arises because the direct and exchange terms are identical.

Using the first-order expression for Γ_2 in Eqs. (24) and (26) yields the following equations of motion:

$$h_b^a \hbar \partial_t \phi_i^b(t) = \zeta_{HFB}^\phi, \tag{44}$$

$$\begin{aligned} \zeta_{HFB}^\phi \equiv &- J[\phi_{i+1}^a(t) + \phi_{i-1}^a(t)] + \frac{U}{\mathcal{N}}[\phi_{id}(t)\phi_i^d(t) \\ &+ G_{iid}^d(t,t)]\phi_i^a(t) + \frac{2U}{\mathcal{N}}[\phi_{ib}(t)G_{ii}^{ab}(t,t)], \end{aligned}$$

$$h_c^a \hbar \partial_t G_{ij}^{cb}(t,t') = \zeta_{HFB}^G,$$

$$\zeta^G_{HFB} \equiv -J[G^{ab}_{i+1j}(t,t') + G^{ab}_{i-1j}(t,t')] + \frac{U}{\mathcal{N}}[\phi_{id}(t)\phi^d_i(t) + G^d_{ii\quad d}(t,t)]G^{ab}_{ij}(t,t') + \frac{2U}{\mathcal{N}}[\phi^a_i(t)\phi_{ic}(t)G^{cb}_{ij}(t,t') + G^a_{ii\quad d}(t,t)G^{db}_{ij}(t,t')] + i\delta^{ab}\delta_{ij}\delta_C(t-t'). \tag{45}$$

In terms of the spectral and statistical functions, Eqs. (39)–(42), and setting $\mathcal{N}=2$, the above equations take the form

$$i\hbar\partial_t\phi_i(t) = -J[\phi_{i+1}(t) + \phi_{i-1}(t)] + U[|\phi_i(t)|^2 + 2\rho^{(F)}_{ii}(t,t)]\phi_i(t) + Um^{(F)}_{ii}(t,t)\phi^*_i(t), \tag{46}$$

$$-i\hbar\frac{\partial}{\partial t}\rho^{(F)}_{ij}(t,t') = \mathbf{L}_{ik}(t)\rho^{(F)}_{kj}(t,t') + \mathbf{M}^*_{ik}(t)m^{(F)}_{kj}(t,t'), \tag{47}$$

$$-i\hbar\frac{\partial}{\partial t}\rho^{(\rho)}_{ij}(t,t') = \mathbf{L}_{ik}(t)\rho^{(\rho)}_{kj}(t,t') + \mathbf{M}^*_{ik}(t)m^{(\rho)}_{kj}(t,t'), \tag{48}$$

$$i\hbar\frac{\partial}{\partial t}m^{(F)}_{ij}(t,t') = \mathbf{L}_{ik}(t)m^{(F)}_{kj}(t,t') + \mathbf{M}_{ik}(t)\rho^{(F)}_{kj}(t,t'), \tag{49}$$

$$i\hbar\frac{\partial}{\partial t}m^{(\rho)}_{ij}(t,t') = \mathbf{L}_{ik}(t)m^{(\rho)}_{kj}(t,t') + \mathbf{M}_{ik}(t)\rho^{(\rho)}_{kj}(t,t'), \tag{50}$$

with

$$\mathbf{L}_{ij}(t) = -J(\delta_{i+1j} + \delta_{i-1j}) + 2U\delta_{ij}(|\phi_i(t)|^2 + \rho^F_{ii}(t,t)), \tag{51}$$

$$\mathbf{M}_{ij}(t) = U\delta_{ij}(\phi_i(t)^2 + m^F_{ii}(t,t)). \tag{52}$$

The time-dependent HFB equations are a closed set of self-consistent equations that describe the coupled dynamics of the condensate and noncondensate components of a Bose gas. It can be checked that they preserve important conservation laws such as the number of particles and energy. The conservation properties of the HFB equations can also be understood by the fact that these equations can also be derived using Gaussian variational methods [7]. These methods always yield a classical Hamiltonian dynamics which guarantees probability conservation. Because they are local in time they can be decoupled by a mode decomposition. (See Appendix A for details.)

VIII. SECOND-ORDER EXPANSION

A. Equations of motion

1. Full second order

The second-order contribution to Γ_2 is described in terms of the setting-sun, Fig. 2(b), and the basketball, Fig. 2(c) diagrams. The basketball diagram is independent of the mean field and is constructed with only quartic vertices. The setting-sun diagram depends on ϕ and contains only three-point vertices. The second-order $\Gamma^{(2)}_2$ effective action can be written as

$$\Gamma^{(2)}_2[\phi,G] = i\left(\frac{U}{\mathcal{N}}\right)^2\int dt_i dt_j \phi_{ib}(t)\phi_{jb'}(t') \times[G^{bb'}_{ij}(t,t')G_{ijdd'}(t,t')G^{dd'}_{ij}(t,t') + 2G^{bd'}_{ij}(t,t')G_{ijdd'}(t,t')G^{db'}_{ij}(t,t')] + i\left(\frac{U}{2\mathcal{N}}\right)^2\int dt_i dt'_j[G_{ijbb'}(t,t')G^{bb'}_{ij}(t,t') \times G_{ijdd'}(t,t')G^{dd'}_{ij}(t,t') + 2 \times G_{ijbb'}(t,t')G^{bd'}_{ij}(t,t')G_{ijdd'}(t,t')G^{db'}_{ij}(t,t')]. \tag{53}$$

To simplify the notation, let us introduce the following definitions [23]:

$$\Pi_{ij}(t,t') = -\frac{1}{2}G_{ijab}(t,t')G^{ab}_{ij}(t,t'), \tag{54}$$

$$\Xi_{ijab}(t,t') = -D(t,t')G_{ijab}(t,t'), \tag{55}$$

$$D(t,t') = \phi_{ib}(t)\phi_{ja}(t')G^{ba}_{ij}(t,t') - \Pi_{ij}(t,t'), \tag{56}$$

$$\overline{\Lambda}^b_{ija}(t,t') = -G^{cb}_{ij}(t,t')G_{ijca}(t,t'), \tag{57}$$

$$\Lambda^b_{ij\ a}(t,t') = -G^{bc}_{ij}(t,t')G_{ijac}(t,t'), \tag{58}$$

$$\Theta^{ac}_{ij}(t,t') = -[\phi_{id}(t)\phi_{jb}(t') + G_{ijdb}(t,t')]G^{ab}_{ij}(t,t')G^{dc}_{ij}(t,t') + \Xi^{ac}_{ij}(t,t'). \tag{59}$$

With the above definitions we find from Eqs. (24) and (26) the following equations of motion:

$$h^a_b\hbar\partial_t\phi^b_i(t) = \zeta^\phi_{HFB} + i\left(\frac{2U}{\mathcal{N}}\right)^2\int dt'_j\phi_{jb}(t')[\Pi_{ij}(t,t')G^{ba}_{ji}(t',t) + \overline{\Lambda}^b_{ijc}(t,t')G^{ac}_{ij}(t,t')], \tag{60}$$

$$h^a_c\hbar\partial_t G^{cb}_{ij}(t,t') = \zeta^G_{HFB} + i\left(\frac{2U}{\mathcal{N}}\right)^2\phi^a_i(t)\int dt''_k\phi_{kc}(t'') \times[\Pi_{ik}(t,t'')G^{cb}_{kj}(t'',t') + \overline{\Lambda}^c_{ik\ d}(t,t'')G^{db}_{kj}(t'',t')] + i\left(\frac{2U}{\mathcal{N}}\right)^2\int dt''[\Theta^a_{ikd}(t,t'') + \Lambda^{ca}_{ik}(t,t')\phi_{ic}(t)\phi_{kd}(t'')]G^{db}_{kj}(t'',t'), \tag{61}$$

where ζ^ϕ_{HFB} and ζ^G_{HFB} are defined in Eq. (45). For explicit expressions in terms of $\rho^{(F,\rho)}$ and $m^{(F,\rho)}$ see Appendix B.

2. 2PI-1/$\mathcal{N}$ expansion

The 2PI effective action is a singlet under $O(\mathcal{N})$ rotations. It can be shown that all graphs contained in an $O(\mathcal{N})$ expansion can be built from the irreducible invariants [23]: ϕ^2, $\mathrm{Tr}(G^n)$, and $\mathrm{Tr}(\phi\phi G^n)$, with $n<\mathcal{N}$. The factors of $\mathcal{N}$ in a single graph contributing to the same $1/\mathcal{N}$ expansion have then two origins: a factor of $\mathcal{N}$ from each irreducible invariant and a factor of $1/\mathcal{N}$ from each vertex. The leading-order large $\mathcal{N}$ approximation scales proportional to $\mathcal{N}$, the NLO contributions are of order 1, and so on. At leading order only the first term of Eq. (44) contributes. At the next-to-leading-order level, if we truncate up to second order in the coupling strength, the double-bubble is totally included but only certain parts of the setting-sun and basketball diagrams are included: the first term in both of the integrals of Eq. (53),

$$\begin{aligned}\Gamma_2^{(2)1/\mathcal{N}}[\phi,G] = i\left(\frac{U}{\mathcal{N}}\right)^2 \int dt_i dt_j \phi_{ib}(t)\phi_{jb'}(t') \\ \times [G_{ij}^{bb'}(t,t')G_{ijdd'}(t,t')G_{ij}^{dd'}(t,t')] \\ + i\left(\frac{U}{2\mathcal{N}}\right)^2 \int dt_i dt_j' [G_{ijbb'}(t,t')G_{ij}^{bb'}(t,t') \\ \times G_{ijdd'}(t,t')G_{ij}^{dd'}(t,t')]. \end{aligned} \tag{62}$$

The equations of motion under this approximation are the ones obtained for the full second-order expansion but with $\Lambda=\bar{\Lambda}=0$, and $\Theta=\Xi$.

In Appendix B we explicitly write the equations of motion in terms of the spectral and statistical functions. We end this section by emphasizing that the only approximation introduced in the derivation of the equations of motion presented here is the truncation up to second order in the interaction strength. These equations depict the nonlinear and non-Markovian quantum dynamics, which we consider as the primary distinguishing features of this work. It supersedes what the second-order kinetic theories currently presented can do, their going beyond the HFB approximation notwithstanding. For example, Ref. [39] presents a kinetic theory approach that includes binary interactions to second order in the interaction potential but uses the Markovian approximation. In Ref. [44] the authors gave a non-Markovian generalization to the quantum kinetic theory derived by Walser *et al.* [8] by including memory effects. However in that work symmetry-breaking fields ϕ and anomalous fluctuations m are neglected.

B. Conservation laws

For a closed (isolated) system the mean total number of particles N and energy are conserved quantities as they are the constants of motion for the dynamical equations.

Particle number conservation is a consequence of the invariance of the Hamiltonian under a global phase change. The mean total number of particles is given by

$$\langle\hat{N}\rangle = \sum_i \langle\hat{\Phi}_i^\dagger\hat{\Phi}_i\rangle = \sum_i \left(|\phi_i|^2 + \rho_{ii}^{(F)} - \frac{1}{2}\right) = N. \tag{63}$$

The kinetic equation for N is then

$$\begin{aligned}\frac{d}{dt}\langle\hat{N}(t)\rangle = \sum_i 2\,\mathrm{Re}\left(\phi_i(t)\frac{\partial}{\partial t}\phi_i^*(t)\right) \\ + \lim_{t\to t'}\left(\frac{\partial}{\partial t}\rho_{ii}^{(F)}(t,t') + \frac{\partial}{\partial t'}\rho_{ii}^{*(F)}(t',t)\right) = 0. \end{aligned} \tag{64}$$

All three approximations we have considered, namely, HFB, $1/\mathcal{N}$ expansion, and full second-order expansion, conserve particle number. This can be shown by plugging in the kinetic equation of $\langle\hat{N}(t)\rangle$ [Eq. (65)] the equation of motion for the mean field and the normal statistical propagator [Eqs. (45) and (46), Eqs. (B3) and (B4), and Eqs. (B10) and (B11)], and canceling terms. It is important to note that even though total population is always conserved there is always a transfer of population between condensate and noncondensate atoms.

While number conservation can be proved explicitly, proving total-energy conservation is not obvious as the Hamiltonian cannot be represented as a linear combination of the relevant operators. It is clear that the exact solution of a closed system is unitary in time and hence disallows any dissipation. However, the introduction of approximation schemes that truncate the infinite hierarchy of correlation functions at some finite order with causal boundary conditions may introduce dissipation [13].

To discuss energy conservation we can use the ϕ-derivable criteria [45] which state that nonequilibrium approximations in which the self-energy Σ is of the form $\delta\Phi/\delta G$, with Φ a functional of G, conserve particle number, energy, and momentum. All the approximations we consider in this paper are ϕ derivable and thus they obey energy, particle number, and momentum conservation laws. For HFB, $\Phi=\Gamma_2^{(1)}$, for the full second-order expansion, $\Phi=\Gamma_2^{(1)}+\Gamma_2^{(2)}$, and for the second-order next-to-leading-order $1/\mathcal{N}$ expansion, $\Phi=\Gamma_2^{(1)}+\Gamma_2^{(2)1/\mathcal{N}}$. See Eqs. (25), (43), (53), and (62). For a detailed discussion of the complete next-to-leading-order $1/\mathcal{N}$ expansion see Refs. [22,23] and references therein.

C. Zero-mode fluctuations

The spectrum of fluctuations above the condensate includes a zero mode. This mode is the Goldstone boson associated with the breaking of global phase invariance by the condensate. It is analogous to the collective modes which arise in the spectrum of fluctuations around a bubble [46]. The zero mode is essentially nonperturbative. In linearized theory, it introduces an artificial infrared divergence in low-dimensional models. For this reason linearized theory is actually improved if the contribution from this mode is neglected altogether [47]. A different way to deal with the zero mode has been proposed by Gardiner [48] and Morgan [30]. Here the theory is written in terms of operators which ex-

change particles between zero and nonzero modes, conserving the total particle number, and one further operator which changes total particle number. The contribution from the zero mode is then subtracted by expressing the normal and anomalous densities in terms of the former alone. However, from a physical point of view the zero mode exists and is quantum in nature. We may think of it as the limit of Gardiner and Zoller's [9] "condensate band " when the width of the band shrinks to zero. There are both fundamental and practical reasons why isolating and subtracting the zero mode is not as compelling in our case as in the problems discussed by Gardiner and Morgan. In the problem we discuss, the initial state is a coherent state rather than a proper state of the total particle number. As the total particle number is not very high quantum fluctuations in the total particle number are real and non-negligible. Discarding these fluctuations would spoil the integrity of the formalism. Also, because the 2PI formalism goes beyond the linearized approximation, the zero mode does not have the impact it has in the linearized formalism and it is not clear that subtracting it necessarily leads to a better approximation. Therefore, in this paper we shall not attempt to isolate the contributions from the zero mode. A full nonperturbative treatment in the future is certainly desirable.

IX. NUMERICAL IMPLEMENTATION

A. Exact solution

The fully quantal solution was found by evolving in time the initial state with the Bose-Hubbard Hamiltonian given by Eq. (1), so that $|\varphi(t)\rangle = e^{-(i/\hbar)\hat{H}t}|\varphi(0)\rangle$ with $|\varphi(0)\rangle = e^{-N/2}e^{\sqrt{N}\hat{\Phi}_0^\dagger}|0\rangle_0 \Pi_{i\neq 0}|0\rangle_i$. To do the numerical calculations we partitioned the Hilbert space in subspaces with fixed number of atoms and propagated independently the projections of the initial state on the respective subspaces. A subspace with N_n number of atoms and I number of wells is spanned by $(N_n + I - 1)!/N_n!(I-1)!$ states. This procedure could be done because the Hamiltonian commutes with the number operator $\Sigma_i \hat{\Phi}_i{}^\dagger \hat{\Phi}_i$, and thus during the dynamics the different subspaces never get mixed. The number of subspaces used for the numerical evolution were such that no change in plots of the dynamical observables was detected by adding another subspace. Generally for N atoms in the initial state, this condition was achieved by including the subspaces between $N - 4\sqrt{N}$ and $N + 4\sqrt{N}$ atoms.

B. Numerical algorithm for the approximated solution

The time-evolution equations obtained in Sec. VIII are nonlinear integro-differential equations. Though the equations are very complicated, they can be solved on a computer. The important point to note is that all equations are causal in time, and all quantities at some later time t_f can be obtained by integration over the explicitly known functions for times $t \leqslant t_f$.

For the numerical solution we employed a time discretization $t = na_t$, $t' = ma_t$, and took the advantage that due to the presence of the lattice the spatial dimension is discrete (indices i and j). The discretized equations for the time evolution of the matrices $\rho_{ijnm}^{(F,\rho)}$, $m_{ijnm}^{(F,\rho)}$, and ϕ_{in} advance time-stepwise in the n direction for fixed m. Due to the symmetries of the matrices only half of the (n,m) matrices have to be computed and the values $\rho_{ijnn}^{\rho} = -i$, $m_{ijnn}^{\rho} = 0$ are fixed for all time due to the bosonic commutation relations. As initial conditions one specifies $\rho_{ij00}^{(F,\rho)}$, $m_{ij00}^{(F,\rho)}$, and ϕ_{i0}.

To ensure that the discretized equations retain the conservation properties present in the continuous ones one has to be very careful in the evolution of the diagonal terms of $\rho_{iinn}^{(F)}$ and take the limit $m \to n$ in a proper way:

$$\rho_{ijn+1n+1}^{(F,\rho)} - \rho_{ijnn}^{(F,\rho)} = (\rho_{ijn+1n}^{(F,\rho)} - \rho_{ijnn}^{(F,\rho)}) \pm (\rho_{jin+1n}^{*(F,\rho)} - \rho_{jinn}^{*(F,\rho)}), \tag{65}$$

$$m_{ijn+1n+1}^{(F,\rho)} - m_{ijnn}^{(F,\rho)} = (m_{ijn+1n}^{(F,\rho)} - m_{ijnn}^{(F,\rho)}) \pm (m_{jin+1n}^{(F,\rho)} - m_{jinn}^{(F,\rho)}), \tag{66}$$

with the positive sign for the statistical propagators, (F)'s and negative for the spectral ones, (ρ)'s. We use the fourth-order Runge-Kutta algorithm to propagate the local part of the equations and a regular one-step Euler method to iterate the nonlocal parts. For the integrals we use the standard trapezoidal rule. Starting with $n=1$, for the time step $n+1$ one computes successively all entries with $m = 0, \ldots, n, n+1$ from known functions evaluated at previous times.

The time step a_t was chosen small enough so that convergence was observed, that is, further decreasing it did not change the results. The greater the parameter UN/J, the smaller is the time step required. The main numerical limitation of the 2PI approximation is set by the time integrals, which make the numerical calculations time and memory consuming. However, within a typical numerical precision it was typically not necessary to keep all the history of the two point functions in the memory. A characteristic time, after which the influence of the early time in the late-time behavior is given by the inverse damping rate. This time is described by the exponential damping of the two-point correlator at time t with the initial time [23]. In our numerics we extended the length of the employed time interval until the results did not depend on it. In general, it was less than the inverse damping rate. We used for the calculations a single PII 400 MHz workstation with 260 Mb of memory. For a typical run 1–2 days of computational time were required.

C. Initial conditions and parameters

To model the patterned loading the initial conditions assumed for the numerical solutions were $\phi_{i0} = N\delta_{i0}$, $\rho_{ij00}^{(F)} = \frac{1}{2}\delta_{ij}$, $\rho_{ij00}^{(\rho)} = -i\delta_{ij}$, and $m_{ij00}^{(F)} = m_{ij00}^{(\rho)} = 0$. They correspond to an initial coherent state with N atoms in the initial populated well.

To study the kinetic-energy dominated regime we chose for the simulations three different sets of parameters: The first set was chosen to be in the very weak interacting regime, $I=3, N=6, J=1$, and $U/J = 1/30$. With this choice we

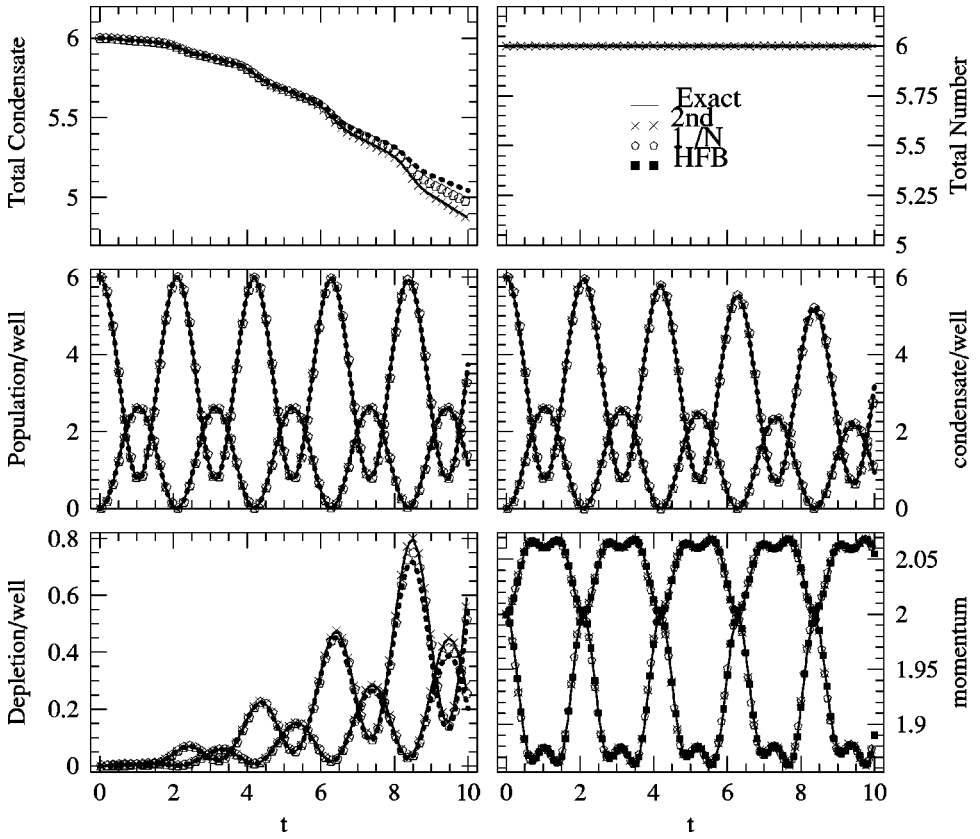

FIG. 3. Comparisons between the exact solution (solid line), the HFB approximation (boxes), the second-order large $\mathcal{N}$ approximation (pentagons), and the full 2PI second-order approximation (crosses) for the very weak interacting regime. The parameters used were $I=3, N=6, J=1$, and $U/J=1/30$. The time is given in units of $\hbar/J$. In the plots where the population, condensate, and depletion per well are depicted the top curves correspond to the initially populated well solutions and the lower to the initially empty wells. Notice the different scale used in the depletion plot. In the momentum distribution plot the upper curve corresponds to the $k=\pm 2\pi/3$ intensities and the lower one to the $k=0$ quasimomentum intensity.

wanted to show the validity of a mean-field approach to describe this regime and the corrections introduced by the higher-order approximations. The second set of parameters were $I=3, N=8, J=1$, and $U/J=1/3$. In this regime the kinetic energy is big enough to allow tunneling but the effect of the interactions are crucial in the dynamics. Comparing with the exact solution we could show the breakdown of the mean-field approximation.

At the mean-field level (using the DNLSE) for a given number of wells, the only relevant parameter for describing the dynamics of the system is the ratio UN/J. For a fixed UN/J the mean-field dynamics is independent of the number of atoms in consideration. This is not the case in the exact solution where both UN/J and N are important. As N is increased, the bigger is the population in the initial coherent matter field and therefore we expect a better agreement of the truncated theories with the exact solution. To study the dependence of the dynamics on the total number of atoms, the third set of parameters in our solutions were chosen to be $I=2, J=1/2$, and fixed $NU/J=4$ but we changed the number of atoms from 20 to 80. To increase the number of atoms in the calculations we had to reduce the number of wells to 2 due to the fact that the dimension of the Hilbert space scales very badly with N and I.

X. RESULTS AND DISCUSSION

In Figs. 3–7 we show our numerical results. We focus our attention on the evolution of the condensate population per well, $|\phi_i(t)|^2$, the total atomic population per well, $|\phi_i|^2 + \rho_{ii}^{(F)}(t,t) - \frac{1}{2}$, the depletion per well or atoms out of the condensate, $\rho_{ii}^{(F)}(t,t) - \frac{1}{2}$, and the total condensate population, $\Sigma_i |\phi_i(t)|^2$. The total population is also explicitly shown in the figures to emphasize number conservation.

The quasimomentum distribution of the atoms released from the lattice is important because it is one of the most easily accessible quantities from an experiment. The quasimomentum distribution function n_k is defined as

$$n_k(t) = \frac{1}{I} \sum_{i,j} e^{ik(i-j)} \langle \Phi_i^\dagger(t) \Phi_j(t) \rangle, \tag{67}$$

where the quasimomentum k can assume discrete values which are integral multiples of $2\pi/Ia$, with I the total number of lattice sites and a the lattice spacing.

The basic features of the plots can be summarized as follows.

(a) *In the very weak interacting regime* (Fig. 3) the dynamics of the atomic population per well resembles the Rabi

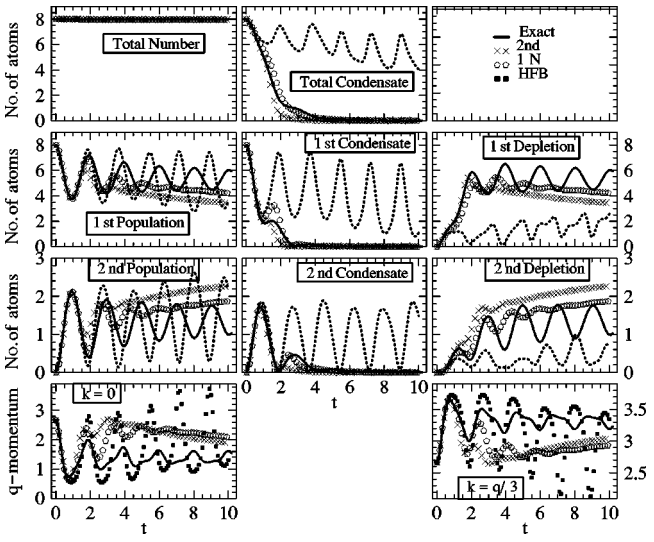

FIG. 4. Comparisons for the case $I=3, N=8, J=1$, and $U/J=1/3$. The time is given in units of $\hbar/J$. In the plots the abbreviation 1st is used for the initially occupied well and 2nd for the initially empty wells. In the quasimomentum plots $q=2\pi/a$ is the reciprocal lattice vector with a the lattice spacing.

oscillation phenomenon. Notice that even though there are three wells, periodic boundary conditions enforce equal evolution of the initial empty ones. In this regime damping effects remain very small for the time depicted in the plots. The numerical simulations show a general agreement between the different approaches with the exact solution. The effect of including higher-order terms in the equations of motion introduce small corrections which improve the agreement with the exact dynamics. This shows up in the plots of the condensate population and depletion, where the small differences can be appreciated better. The second-order $1/\mathcal{N}$ expansion gives an improvement over the HFB and the complete second-order perturbative expansion almost matches perfectly with the exact solution. In the duration depicted in the plots of Fig. 3 the total condensate constitutes an important fraction of the total population. Regarding the quasimomentum distribution we observe that similar to the spatial distribution where the initial configuration and periodic boundary conditions reduce the three-well system to a double-well one, they enforce equal evolution of the $\pm 2\pi/3$ quasimomentum intensities. The $k=0$ and $\pm 2\pi/3$ intensities oscillate with the same frequency as the atomic population per well, both are also well described by the approximations in consideration.

(b) *In the intermediate regime* we can see the effect of the interactions in the dynamics. They modulate the oscillations in the population per well and scatter the atoms out of the condensate.

(c) In Fig. 4 we plot the numerical solution for the parameters $I=3, N=8, J=1$, and $U/J=1/3$. In contrast to the case of the very weak interacting regime, it is only at very early times that any of these approximations is close to the exact solution. Even though none of them are good after the first oscillation, the HFB approximation is the only one that fails to capture the exponential decrease of the condensate population. This is expected, because even though this approximation goes beyond mean-field theory and takes into account the most important scattering effects, it includes the effects of collisions only indirectly through energy shifts, and breaks down outside the collisionless regime where multiple-scattering effects are important. In contrast, the exponential decay of the condensate is present in the second-order approximations. Nonlocal parts of the self-energy included in them encode scattering effects responsible for damping. It is important to point out that, even though we observe the collapse of the condensate population, the total population is always conserved: As the condensate population decreases, the number of atoms out of the condensate increases.

(2) Comparing the two second-order approaches we observe that the full second-order expansion gives a better description of the dynamics than the $1/\mathcal{N}$ solution only in the regime where the perturbative solutions are close to the exact

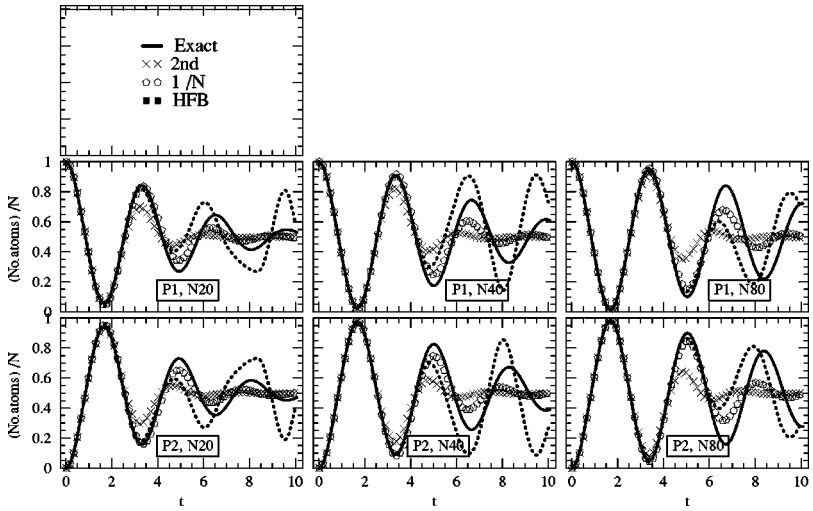

FIG. 5. Comparison between the evolution of the atomic population per well for $I=2, J=1/2, NU/J=4$, and $N=20, 40$, and 80. Time is in units $\hbar/J$. In the plots P1 stands for the fractional atomic population in the initially populated wells and P2 for the population in the initially empty wells. The number of atoms N is explicitly shown in each panel.

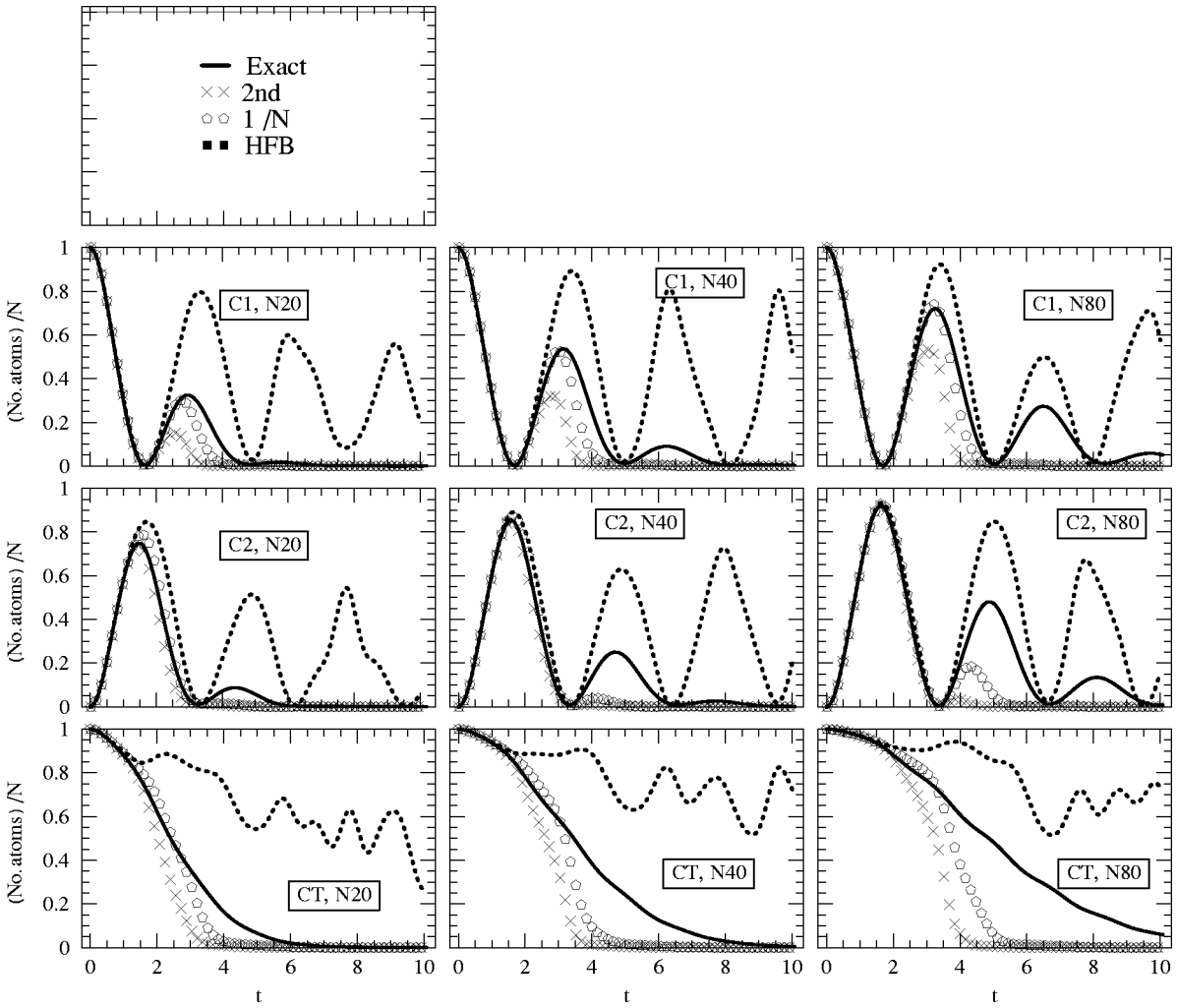

FIG. 6. Time evolution of the condensate population per well and the total condensate population, for the same parameters as in Fig. 5. Time is in units of $\hbar/J$. In the plots C1 stands for the fractional condensate population in the initially populated well, C2 for the fractional condensate population in the initially empty one, and CT for the total condensate fraction.

dynamics. As soon as the third-order terms start to be important, the large $1/\mathcal{N}$ expansion gives a better qualitative description. This behavior is going to be appreciated better in Figs. 5–7 as the number of atoms is increased (see discussion below).

We observe as a general issue in this regime that, regardless of the fact that the second-order solutions capture the damping effects, as soon as the condensate population decreases to a small percentage of the total population, they depart from the exact dynamics: the second-order approaches predict faster damping rates. The overdamping is more severe in the dynamics of the population per well than in the condensate dynamics. The failure can be understood under the following lines of reasoning. At zero temperature condensate atoms represent the most "classical" form of a matter wave. When they decay, the role of quantum correlations become more important. At this point the higher-order terms neglected in the second-order approximations are the ones that lead the dynamical behavior. Thus, to have a more accurate description of the dynamics after the coherent matter field has decayed, one needs a better treatment of correlations.

Damping effects are also quite noticeable in the quantum evolution of the quasimomentum intensities. Similar to what happens to the spatial observables, the HFB approximation fails completely to capture the damping effects present in the evolution of the Fourier intensities whereas the second-order approaches overestimate them.

(3) In Figs. 5–7 we explore the effect of the total number of atoms on the dynamics. In the plots we show the numerical solutions found for a double-well system with fixed ratio $UN/J=4$ and three different values of $N, N=20, 40$, and 80. We present the results obtained for the evolution of the atomic population per well in Fig. 5, the condensate population per well and total condensate population in Fig. 6, and the quasimomentum intensities in Fig. 7. To make the comparisons easier we scaled the numerical results obtained for the three different values of N by dividing them by the total number of atoms. In this way for all the cases we start with an atomic population of magnitude one in the initial populated well. In the exact dynamics we see that as the number of atoms is increased the damping effects occur at slower rates. This feature can be noticed in the quantum dynamics of all the observables depicted in Figs. 5–7. The decrease of

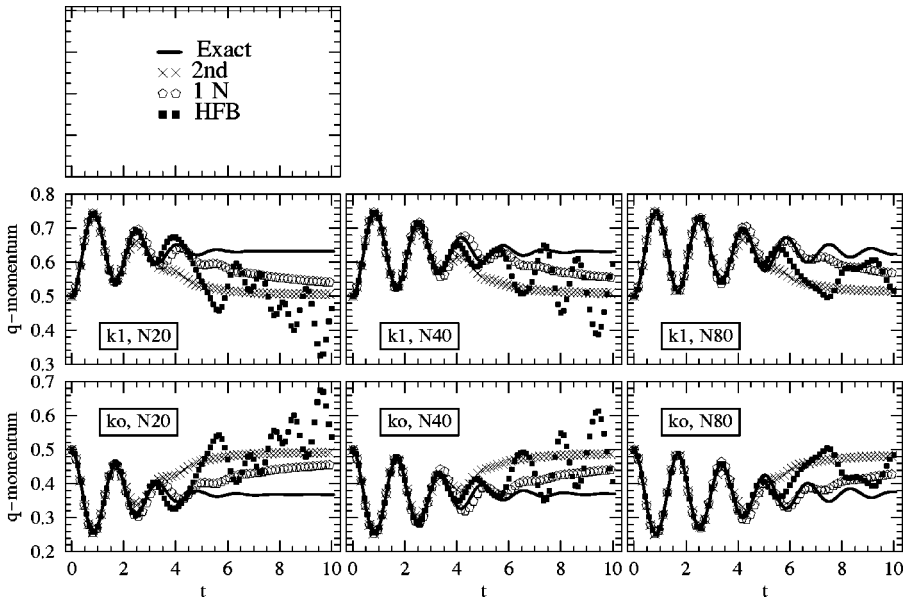

FIG. 7. Dynamical evolution of the quasimomentum intensities. The parameters used were $I=2, J=1/2, NU/J=4$, and $N=20, 40$, and 80. Time is in units of $\hbar/J$. In the plots ko denotes the $k=0$ quasimomentum component and k1 the $k=\pi/a$ one (a the lattice spacing). The plots are scaled to set the integrated quasimomentum density to one for all N.

the damping rates as the number of atoms is increased is not surprising because by changing the number of atoms we affect the quantum coherence properties of the system. As comment in Sec. III the collapse time of the condensate population is approximately given by $t_{coll} \sim t_{rev}/2\pi\sqrt{N}$. The revival time is proportional to U^{-1} and varies with N for fixed UN/J as $t_{rev} \propto N/J$, thus $t_{coll} \propto \sqrt{N}$ increases with N as observed in the numerical calculations. Besides damping rates, the qualitative behavior of the exact quantum dynamics is not affected very much as the number of atoms is increased for a fixed UN/J.

The improvement of the 2PI approximations as N is increased, as a result of the increase in the initial number of coherent atoms, is in fact observed in the plots. Even though the problem of underdamping in the HFB approximation and overdamping in the second-order approaches are not cured, as the number of atoms is increased, we do observe a better matching with the full quantal solution. The $1/\mathcal{N}$ expansion shows the fastest convergence. Perhaps this issue can be more easily observed in the quasimomentum distribution plots, Fig. 7. The better agreement of the $1/\mathcal{N}$ expansion relies on the fact that even though the number of fields is only 2 in our calculations, the $1/\mathcal{N}$ expansion is an expansion about a strong quasiclassical field configuration.

XI. CONCLUSIONS

In this work we have used the CTP functional formalism for 2PI Green's functions to describe the nonequilibrium dynamics of a condensate loaded in an optical lattice on every third lattice site. We have carried out the analysis up to second order in the interaction strength. This approximation is introduced so as to make the numerical solution manageable, but it is sufficient to account for dissipative effects due to multiparticle scattering that are crucial even at early times. Our formulation is capable of capturing the salient features of the system dynamics in the regime under consideration, such as the decay of the condensate population and the damping of the oscillations of the quasimomentum and population per well unaccounted for in the HFB approximation. However, at the point where an important fraction of the condensate population has been scattered out, the second-order approximations used here predict an overdamped dynamics. To improve on this a better treatment of higher correlations is required. One might try to include the full next-to-leading-order large $\mathcal{N}$ expansion without the truncation to second order as done in Ref. [23] but it is not obvious that this will lead to the required improvement. Alternatively, one may try to adopt a stochastic approach, but the challenge will be shifted to the derivation of a noise term (which is likely to be both colored and multiplicative) which contains the effects of these higher correlations and the solution of the stochastic equations. We hope to address this aspect of the problem in a future work.

Even though, as is clear in this paper, the second-order 2PI approximations fail to capture the fully correlated dynamics in the system, it has been proved to work at intermediate times when correlations are not negligible and standard mean-field techniques fail poorly. Because of its success in describing moderately correlated regimes, the second-order approximations could become a useful tool for describing experimental situations as the collapsing or colliding condensate experiments [4] where striking dynamical behavior such as collisional loss of condensate atoms has been observed.

In summary, we have presented an approach for the description of the nonequilibrium dynamics of a Bose-Einstein condensate and fluctuations in a closed quantum field system. The formalism allows one to go beyond the well-known HFB approximation and to incorporate the nonlinear and non-Markovian aspects of the quantum dynamics as manifest

in the dissipation and fluctuations phenomena. The 2PI effective action formalism provides a useful framework where the mean field and the correlation functions are treated on the same footing self-consistently and that respects conservation of particle number and energy. The CTP formalism ensures that the dynamical equations of motion are also causal. In their current form the scattering terms are nonlocal in time, are hard to estimate analytically, and their calculation is numerically demanding. However, this systematic approach can be used as a quantitative means to obtain solutions in different regimes and make comparisons with kinetic theory results where a Markovian approximation is assumed. We have not made such comparisons in this work, but a future test of the consequences of the Markovian assumption would be of great interest.

ACKNOWLEDGMENTS

A.M.R. acknowledges correspondence with Dr. Berges on his recent large $\mathcal{N}$ numerical results and discussions with Ted Kirkpatrick. A.M.R. and C.C. were supported in part by an Advanced Research and Development Activity contract and by the U.S. National Science Foundation under Grant No. PHY-0100767. B.L.H. and the visits of E.C. were supported in part by a NSF grant, a NIST grant, and an ARDA contract. E.C. was supported by the University of Buenos Aires, CONICET, Fundacion Antorchas, and ANPCyT under Project No. PICT 99 03-05229. A.R. was supported by NSF under Grant No. PHY-0300710.

APPENDIX A: MODE EXPANSION OF THE HFB EQUATIONS

To decouple the HFB equations we apply the well-known Bogoliubov transformation to the fluctuation field:

$$\varphi_j(t) = \sum_q u_i^q(t)\hat{\alpha}_q - v_i^{*q}(t)\hat{\alpha}_q^\dagger, \tag{A1}$$

where $(\hat{\alpha}_q, \hat{\alpha}_q^\dagger)$ are time-independent creation and annihilation quasiparticle operators and all the time dependence is absorbed in the amplitudes $\{u_i^q(t), v_i^{*q}(t)\}$. To ensure that the quasiparticle transformation is canonical, the amplitudes $\{u_i^q(t), v_i^{*q}(t)\}$ have to fulfill the following relations [49]:

$$\sum_i u_i^q(t)u_i^{*k}(t) - v_i^q(t)v_i^{*k}(t) = \delta_{qk}, \tag{A2}$$

$$\sum_i u_i^q(t)v_i^k(t) - v_i^q(t)u_i^k(t) = 0. \tag{A3}$$

In the zero-temperature limit, where $\langle\hat{\alpha}_q^\dagger\hat{\alpha}_k\rangle = 0$, the statistical and spectral functions take the form

$$\rho_{ij}^{(F)}(t,t') = \frac{1}{2}\sum_q [v_i^q(t)v_j^{*q}(t') + u_j^q(t')u_i^{*q}(t)], \tag{A4}$$

$$\rho_{ij}^{(\rho)}(t,t') = i\sum_q [v_i^q(t)v_j^{*q}(t') - u_j^q(t')u_i^{*q}(t)], \tag{A5}$$

$$m_{ij}^{(F)}(t,t') - \frac{1}{2}\sum_q [u_i^q(t)v_j^{*q}(t') + u_j^q(t')v_i^{*q}(t)], \tag{A6}$$

$$m_{ij}^{(\rho)}(t,t') - i\sum_q [u_i^q(t)v_j^{*q}(t') - u_j^q(t')v_i^{*q}(t)]. \tag{A7}$$

Replacing Eqs. (A4)–(A7) by Eqs. (46)–(50) and using the constraints (A2) and (A3) we recover the standard time-dependent equations for the quasiparticle amplitudes [7]:

$$i\hbar\partial_t\phi_i(t) = -J[\phi_{i+1}(t) + \phi_{i-1}(t)] + U[|\phi_i(t)|^2 + 2\rho_{ii}^{(F)}(t,t)]\phi_i(t) + Um_{ii}^{(F)}(t,t)\phi_i^*(t), \tag{A8}$$

$$i\hbar\frac{\partial}{\partial t}u_i^q(t) = -J[u_{i+1}^q(t) + u_{i-1}^q(t)] + 2U[|\phi_i(t)|^2 + \rho_{ii}^{(F)}(t,t)]u_i^q(t) - U[m_{ii}^{(F)}(t,t) + \phi_i(t)^2]v_i^q(t), \tag{A9}$$

$$-i\hbar\frac{\partial}{\partial t}v_i^q(t) = -J[v_{i+1}^q(t) + v_{i-1}^q(t)] + 2U[|\phi_i(t)|^2 + \rho_{ii}^{(F)}(t,t)]v_i^q(t) - U[m_{ii}^{*(F)}(t,t) + \phi_i(t)^{*2}]u_i^q(t). \tag{A10}$$

Equations (A8)–(A10) correspond to a set of $I(2I+1)$ coupled ordinary differential equations, where I is the total number of lattice sites. They can be solved using standard time propagation algorithms. Once the time-dependent quasiparticle amplitudes are calculated we can derive the dynamics of physical observables constructed from them as a function of time, such as the average number of particles in a well, $n_i(t)$, etc.

APPENDIX B: SECOND-ORDER EQUATIONS OF MOTION

Here we explicitly write the equations of motion of the $1/\mathcal{N}$ and full second-order approximations.

To simplify the notation let us introduce the functions

$$\Omega_{ij}^{(F)}[\mathbf{f},\mathbf{g}] = \mathbf{f}_{ij}^{(F)}(t_i,t_j)\mathbf{g}_{ij}^{(F)}(t_i,t_j) - \frac{1}{4}[\mathbf{f}_{ij}^{(\rho)}(t_i,t_j)\mathbf{g}_{ij}^{(\rho)}(t_i,t_j)], \tag{B1}$$

$$\Omega_{ij}^{(\rho)}[\mathbf{f},\mathbf{g}] = \mathbf{f}_{ij}^{(F)}(t_i,t_j)\mathbf{g}_{ij}^{(\rho)}(t_i,t_j) + \mathbf{f}_{ij}^{(\rho)}(t,t')\mathbf{g}_{ij}^{(F)}(t_i,t_j). \tag{B2}$$

Using the spectral and statistical functions and setting $\mathcal{N}$ equal to 2 the equations of motion derived in Sec. VII can be written as follows:

(1) Full second-order expansion: If we take the complete contribution of the setting-sun and basketball diagrams, the equations of motion take the form

$$i\hbar\partial_{t_i}\phi_i = -J[\phi_{i+1}(t_i)+\phi_{i-1}(t_i)]+U(|\phi_i|^2+2\rho_{ii}^{(F)})\phi_i+Um_{ii}^{(F)}\phi_i^*-2U^2\sum_k\int_0^{t_i}dt_k(\phi_k\Omega_{ik}^{(\rho)}[\rho,\rho^*]+\phi_k\Omega_{ik}^{(\rho)}[m,m^*]+\phi_k^*\Omega_{ik}^{(\rho)}$$
$$\times[m,\rho])\rho_{ki}^{(F)}-2U^2\sum_k\int_0^{t_i}(\phi_k^*\Omega_{ik}^{(\rho)}[\rho,\rho^*]+\phi_k^*\Omega_{ik}^{(\rho)}[m,m^*]+\phi_k\Omega_{ik}^{(\rho)}[m^*,\rho^*])m_{ki}^{(F)}+2U^2\sum_k\int_0^{t_i}dt_k(\phi_k\Omega_{ik}^{(F)}[\rho,\rho^*]+\phi_k\Omega_{ik}^{(F)}$$
$$\times[m,m^*]+\phi_k^*\Omega_{ik}^{(F)}[m,\rho])\rho_{ki}^{(\rho)}+2U^2\sum_k\int_0^{t_i}(\phi_k^*\Omega_{ik}^{(F)}[\rho,\rho^*]+\phi_k^*\Omega_{ik}^{(F)}[m,m^*]+\phi_k\Omega_{ik}^{(F)}[m^*,\rho^*])m_{ki}^{(\rho)}, \tag{B3}$$

$$-i\hbar\partial_{t_i}\rho_{ij}^{(F)} = -J[\rho_{i+1j}^{(F)}(t_i,t_j)+\rho_{i-1j}^{(F)}(t_i,t_j)]+2U(|\phi_i|^2+\rho_{ii}^{(F)})\rho_{ij}^{(F)}+U(m_{ii}^{*(F)}+\phi_i^{*2})m_{ij}^{(F)}-2U^2\sum_k\int_0^{t_i}dt_k(\phi_i\phi_k^*\Omega_{ik}^{(\rho)}[\rho,\rho]+2\phi_i\phi_k\Omega_{ik}^{(\rho)}$$
$$\times[\rho,m^*]+2\phi_i^*\phi_k^*\Omega_{ik}^{(\rho)}[m,\rho])\rho_{kj}^{(F)}-2U^2\sum_k\int_0^{t_i}dt_k\{\Omega_{ik}^{(\rho)}[\rho,\Delta]+2\phi_i^*\phi_k(\Omega_{ik}^{(\rho)}[\rho,\rho^*]+\Omega_{ik}^{(\rho)}[m,m^*])\}\rho_{kj}^{(F)}$$
$$-2U^2\sum_k\int_0^{t_i}dt_k(2\phi_i\phi_k^*\Omega_{ik}^{(\rho)}[m^*,\rho]+\phi_i\phi_k\Omega_{ik}^{(\rho)}[m^*,m^*]+2\phi_i^*\phi_k\Omega_{ik}^{(\rho)}[\rho^*,m^*])m_{kj}^{(F)}-2U^2\sum_k\int_0^{t_i}dt_k\{\Omega_{ik}^{(\rho)}[m^*,\Upsilon]$$
$$+\phi_i^*\phi_k^*(2\Omega_{ik}^{(\rho)}[\rho,\rho^*]+2\Omega_{ik}^{(\rho)}[m,m^*])\}m_{kj}^{(F)}+2U^2\sum_k\int_0^{t_j}dt_k(\phi_i\phi_k^*\Omega_{ik}^{(F)}[\rho,\rho]+2\phi_i\phi_k\Omega_{ik}^{(F)}[\rho,m^*]+2\phi_i^*\phi_k^*\Omega_{ik}^{(F)}$$
$$\times[m,\rho])\rho_{kj}^{(\rho)}+2U^2\sum_k\int_0^{t_j}dt_k\{\Omega_{ik}^{(F)}[\rho,\Delta]+2\phi_i^*\phi_k(\Omega_{ik}^{(F)}[\rho,\rho^*]+\Omega_{ik}^{(F)}[m,m^*])\}\rho_{kj}^{(\rho)}+2U^2\sum_k\int_0^{t_j}dt_k(2\phi_i\phi_k^*\Omega_{ik}^{(F)}[m^*,\rho]$$
$$+\phi_i\phi_k\Omega_{ik}^{(F)}[m^*,m^*]+2\phi_i^*\phi_k\Omega_{ik}^{(F)}[\rho^*,m^*])m_{kj}^{(\rho)}+2U^2\sum_k\int_0^{t_j}dt_k\{\Omega_{ik}^{(F)}[m^*,\Upsilon]+2\phi_i^*\phi_k^*(\Omega_{ik}^{(F)}[\rho,\rho^*]+\Omega_{ik}^{(F)}[m,m^*])\}m_{kj}^{(F)}, \tag{B4}$$

$$-i\hbar\partial_{t_i}\rho_{ij}^{(\rho)} = -J[\rho_{i+1j}^{(\rho)}(t_i,t_j)+\rho_{i-1j}^{(\rho)}(t_i,t_j)]+2U(|\phi_i|^2+\rho_{ii}^{(F)})\rho_{ij}^{(\rho)}+U(m_{ii}^{*(F)}+\phi_i^{*2})m_{ij}^{(\rho)}-2U^2\sum_k\int_{t_j}^{t_i}dt_k(\phi_i\phi_k^*\Omega_{ik}^{(\rho)}[\rho,\rho]+2\phi_i\phi_k\Omega_{ik}^{(\rho)}$$
$$\times[\rho,m^*]+2\phi_i^*\phi_k^*\Omega_{ik}^{(\rho)}[m,\rho])\rho_{kj}^{(\rho)}-2U^2\sum_k\int_{t_j}^{t_i}dt_k\{\Omega_{ik}^{(\rho)}[\rho,\Delta]+2\phi_i^*\phi_k(\Omega_{ik}^{(\rho)}[\rho,\rho^*]+\Omega_{ik}^{(\rho)}[m,m^*])\}\rho_{kj}^{(\rho)}$$
$$-2U^2\sum_k\int_{t_j}^{t_i}dt_k(2\phi_i\phi_k^*\Omega_{ik}^{(\rho)}[m^*,\rho]+\phi_i\phi_k\Omega_{ik}^{(\rho)}[m^*,m^*]+2\phi_i^*\phi_k\Omega_{ik}^{(\rho)}[\rho^*,m^*])m_{kj}^{(\rho)}-2U^2\sum_k\int_{t_j}^{t_i}dt_k\{\Omega_{ik}^{(\rho)}[m^*,\Upsilon]$$
$$+2\phi_i^*\phi_k^*(\Omega_{ik}^{(\rho)}[\rho,\rho^*]+\Omega_{ik}^{(\rho)}[m,m^*])\}m_{kj}^{(\rho)}, \tag{B5}$$

$$i\hbar\partial_{t_i}m_{ij}^{(F)} = -J[m_{i+1j}^{(F)}(t_i,t_j)+m_{i-1j}^{(F)}(t_i,t_j)]+2U(|\phi_i|^2+\rho_{ii}^{(F)})m_{ij}^{(F)}+U(m_{ii}^{(F)}+\phi_i^2)\rho_{ij}^{(F)}-2U^2\sum_k\int_0^{t_i}dt_k(2\phi_i^*\phi_k\Omega_{ik}^{(\rho)}[m,\rho^*]+\phi_i^*\phi_k^*\Omega_{ik}^{(\rho)}$$
$$\times[m,m]+2\phi_i\phi_k^*\Omega_{ik}^{(\rho)}[\rho,m])\rho_{kj}^{(F)}-2U^2\sum_k\int_0^{t_i}dt_k\{\Omega_{ik}^{(\rho)}[m,\Upsilon]+2\phi_i\phi_k(\Omega_{ik}^{(\rho)}[\rho,\rho^*]+\Omega_{ik}^{(\rho)}[m,m^*])\}\rho_{kj}^{(F)}$$
$$-2U^2\sum_k\int_0^{t_i}dt_k(\phi_i^*\phi_k\Omega_{ik}^{(\rho)}[\rho^*,\rho^*]+2\phi_i^*\phi_k^*\Omega_{ik}^{(\rho)}[\rho^*,m]+2\phi_i\phi_k\Omega_{ik}^{(\rho)}[m^*,\rho^*])m_{kj}^{(F)}-2U^2\sum_k\int_0^{t_i}dt_k\{\Omega_{ik}^{(\rho)}[\rho^*,\Delta]$$
$$+2\phi_i\phi_k^*(\Omega_{ik}^{(\rho)}[\rho,\rho^*]+\Omega_{ik}^{(\rho)}[m,m^*])\}m_{kj}^{(F)}+2U^2\sum_k\int_0^{t_j}dt_k(2\phi_i^*\phi_k\Omega_{ik}^{(F)}[m,\rho^*]+\phi_i^*\phi_k^*\Omega_{ik}^{(F)}[m,m]+2\phi_i\phi_k^*\Omega_{ik}^{(F)}[\rho,m])\rho_{kj}^{(\rho)}$$
$$+2U^2\sum_k\int_0^{t_j}dt_k\{\Omega_{ik}^{(F)}[m,\Upsilon]+2\phi_i\phi_k(\Omega_{ik}^{(F)}[\rho,\rho^*]+\Omega_{ik}^{(F)}[m,m^*])\}\rho_{kj}^{(\rho)}+2U^2\sum_k\int_0^{t_j}dt_k(\phi_i^*\phi_k\Omega_{ik}^{(F)}[\rho^*,\rho^*]+2\phi_i^*\phi_k^*\Omega_{ik}^{(F)}$$
$$\times[\rho^*,m]+2\phi_i\phi_k\Omega_{ik}^{(F)}[m^*,\rho^*])m_{kj}^{(\rho)}+2U^2\sum_k\int_0^{t_j}dt_k\{\Omega_{ik}^{(F)}[\rho^*,\Delta]+2\phi_i\phi_k^*(\Omega_{ik}^{(F)}[\rho,\rho^*]+\Omega_{ik}^{(F)}[m,m^*])\}m_{kj}^{(\rho)}, \tag{B6}$$

$$i\hbar\partial_{t_i}m_{ij}^{(\rho)} = -J(m_{i+1j}^{(\rho)}(t_i,t_j) + m_{i-1j}^{(\rho)}(t_i,t_j)) + 2U(|\phi_i|^2 + \rho_{ii}^{(F)})m_{ij}^{(\rho)} + U(m_{ii}^{(F)} + \phi_i^2)\rho_{ij}^{(\rho)} + 2U^2\sum_k \int_{t_j}^{t_i} dt_k(2\phi_i^*\phi_k\Omega_{ik}^{(\rho)}[m,\rho^*] + \phi_i^*\phi_k^*\Omega_{ik}^{(\rho)}$$
$$\times[m,m] + 2\phi_i\phi_k^*\Omega_{ik}^{(\rho)}[\rho,m])\rho_{kj}^{(\rho)} + 2U^2\sum_k \int_{t_j}^{t_i} dt_k\{\Omega_{ik}^{(\rho)}[m,\Upsilon] + \phi_i\phi_k(2\Omega_{ik}^{(\rho)}[\rho,\rho^*] + 2\Omega_{ik}^{(\rho)}[m,m^*])\}\rho_{kj}^{(\rho)}$$
$$+ 2U^2\sum_k \int_{t_j}^{t_i} dt_k(\phi_i^*\phi_k\Omega_{ik}^{(\rho)}[\rho^*,\rho^*] + 2\phi_i^*\phi_k^*\Omega_{ik}^{(\rho)}[\rho^*,m] + 2\phi_i\phi_k\Omega_{ik}^{(\rho)}[m^*,\rho^*])m_{kj}^{(\rho)} + 2U^2\sum_k \int_{t_j}^{t_i} dt_k\{\Omega_{ik}^{(\rho)}[\rho^*,\Delta]$$
$$+ 2\phi_i\phi_k^*(\Omega_{ik}^{(\rho)}[\rho,\rho^*] + \Omega_{ik}^{(\rho)}[m,m^*])\}m_{kj}^{(\rho)}, \tag{B7}$$

with

$$\Delta_{ij}^{(F,\rho)} = \Omega_{ij}^{(F,\rho)}[\rho,\rho^*] + 2\Omega_{ij}^{(F,\rho)}[m,m^*], \tag{B8}$$

$$\Upsilon_{ij}^{(F,\rho)} = 2\Omega_{ij}^{(F,\rho)}[\rho,\rho^*] + \Omega_{ij}^{(F,\rho)}[m,m^*]. \tag{B9}$$

Second-order $1/\mathcal{N}$ expansion:

$$i\hbar\partial_{t_i}\phi_i = -J[\phi_{i+1}(t_i) + \phi_{i-1}(t_i)] + U(|\phi_i|^2 + 2\rho_{ii}^{(F)})\phi_i + Um_{ii}^{(F)}\phi_i^* - U^2\sum_k \int_0^{t_i} dt_k\Pi_{ik}^{(\rho)}(\phi_k\rho_{ki}^{(F)} + \phi_k^*m_{ki}^{(F)})$$
$$+ U^2\sum_k \int_0^{t_i} dt_k\Pi_{ik}^{(F)}(\phi_k\rho_{ki}^{(\rho)} + \phi_k^*m_{ki}^{(\rho)}), \tag{B10}$$

$$-i\hbar\partial_{t_i}\rho_{ij}^{(F)} = -J[\rho_{i+1j}^{(F)}(t_i,t_j) + \rho_{i-1j}^{(F)}(t_i,t_j)] + 2U(|\phi_i|^2 + \rho_{ii}^{(F)})\rho_{ij}^{(F)} + U(m_{ii}^{*(F)} + \phi_i^{*2})m_{ij}^{(F)} - U^2\sum_k \int_0^{t_i} dt_k(\phi_i\phi_k^*\Omega_{ik}^{(\rho)}[\rho,\rho] + \phi_i\phi_k\Omega_{ik}^{(\rho)}$$
$$\times[\rho,m^*] + \phi_i^*\phi_k^*\Omega_{ik}^{(\rho)}[m,\rho])\rho_{kj}^{(F)} - U^2\sum_k \int_0^{t_i} dt_k\{\Omega_{ik}^{(\rho)}[\rho,\Pi] + \phi_i^*\phi_k(2\Omega_{ik}^{(\rho)}[\rho,\rho^*] + \Omega_{ik}^{(\rho)}[m,m^*])\}\rho_{kj}^{(F)}$$
$$- U^2\sum_k \int_0^{t_i} dt_k(\phi_i\phi_k^*\Omega_{ik}^{(\rho)}[m^*,\rho] + \phi_i\phi_k\Omega_{ik}^{(\rho)}[m^*,m^*] + \phi_i^*\phi_k\Omega_{ik}^{(\rho)}[\rho^*,m^*])m_{kj}^{(F)} - U^2\sum_k \int_0^{t_i} dt_k\{\Omega_{ik}^{(\rho)}[m^*,\Pi] + \phi_i^*\phi_k^*(\Omega_{ik}^{(\rho)}$$
$$\times[\rho,\rho^*] + 2\Omega_{ik}^{(\rho)}[m,m^*])\}m_{kj}^{(F)} + U^2\sum_k \int_0^{t_j} dt_k(\phi_i\phi_k^*\Omega_{ik}^{(F)}[\rho,\rho] + \phi_i\phi_k\Omega_{ik}^{(F)}[\rho,m^*] + \phi_i^*\phi_k^*\Omega_{ik}^{(F)}[m,\rho])\rho_{kj}^{(\rho)}$$
$$+ U^2\sum_k \int_0^{t_j} dt_k\{\Omega_{ik}^{(F)}[\rho,\Pi] + \phi_i^*\phi_k(2\Omega_{ik}^{(F)}[\rho,\rho^*] + \Omega_{ik}^{(F)}[m,m^*])\}\rho_{kj}^{(\rho)} + U^2\sum_k \int_0^{t_j} dt_k(\phi_i\phi_k^*\Omega_{ik}^{(F)}[m^*,\rho] + \phi_i\phi_k\Omega_{ik}^{(F)}$$
$$\times[m^*,m^*] + \phi_i^*\phi_k\Omega_{ik}^{(F)}[\rho^*,m^*])m_{kj}^{(\rho)} + U^2\sum_k \int_0^{t_j} dt_k\{\Omega_{ik}^{(F)}[m^*,\Pi] + \phi_i^*\phi_k^*(\Omega_{ik}^{(F)}[\rho,\rho^*] + 2\Omega_{ik}^{(F)}[m,m^*])\}m_{kj}^{(F)}, \tag{B11}$$

$$-i\hbar\partial_{t_i}\rho_{ij}^{(\rho)} = -J[\rho_{i+1j}^{(\rho)}(t_i,t_j) + \rho_{i-1j}^{(\rho)}(t_i,t_j)] + 2U(|\phi_i|^2 + \rho_{ii}^{(F)})\rho_{ij}^{(\rho)} + U(m_{ii}^{*(F)} + \phi_i^{*2})m_{ij}^{(\rho)} - U^2\sum_k \int_{t_j}^{t_i} dt_k(\phi_i\phi_k^*\Omega_{ik}^{(\rho)}[\rho,\rho] + \phi_i\phi_k\Omega_{ik}^{(\rho)}$$
$$\times[\rho,m^*] + \phi_i^*\phi_k^*\Omega_{ik}^{(\rho)}[m,\rho])\rho_{kj}^{(\rho)} - U^2\sum_k \int_{t_j}^{t_i} dt_k\{\Omega_{ik}^{(\rho)}[\rho,\Pi] + \phi_i^*\phi_k(2\Omega_{ik}^{(\rho)}[\rho,\rho^*] + \Omega_{ik}^{(\rho)}[m,m^*])\}\rho_{kj}^{(\rho)}$$
$$- U^2\sum_k \int_{t_j}^{t_i} dt_k(\phi_i\phi_k^*\Omega_{ik}^{(\rho)}[m^*,\rho] + \phi_i\phi_k\Omega_{ik}^{(\rho)}[m^*,m^*] + \phi_i^*\phi_k\Omega_{ik}^{(\rho)}[\rho^*,m^*])m_{kj}^{(\rho)} - U^2\sum_k \int_{t_j}^{t_i} dt_k\{\Omega_{ik}^{(\rho)}[m^*,\Pi] + \phi_i^*\phi_k^*(\Omega_{ik}^{(\rho)}$$
$$\times[\rho,\rho^*] + 2\Omega_{ik}^{(\rho)}[m,m^*])\}m_{kj}^{(\rho)}, \tag{B12}$$

$$i\hbar\partial_{t_i} m_{ij}^{(F)} = -J[m_{i+1j}^{(F)}(t_i,t_j) + m_{i-1j}^{(F)}(t_i,t_j)] + 2U(|\phi_i|^2 + \rho_{ii}^{(F)})m_{ij}^{(F)} + U(m_{ii}^{(F)} + \phi_i^2)\rho_{ij}^{(F)} - U^2\sum_k \int_0^{t_i} dt_k(\phi_i^*\phi_k\Omega_{ik}^{(\rho)}[m,\rho^*] + \phi_i^*\phi_k^*\Omega_{ik}^{(\rho)}$$
$$\times[m,m] + \phi_i\phi_k^*\Omega_{ik}^{(\rho)}[\rho,m])\rho_{kj}^{(F)} - U^2\sum_k \int_0^{t_i} dt_k\{\Omega_{ik}^{(\rho)}[m,\Pi] + \phi_i\phi_k(\Omega_{ik}^{(\rho)}[\rho,\rho^*] + 2\Omega_{ik}^{(\rho)}[m,m^*])\}\rho_{kj}^{(F)}$$
$$- U^2\sum_k \int_0^{t_i} dt_k(\phi_i^*\phi_k\Omega_{ik}^{(\rho)}[\rho^*,\rho^*] + \phi_i^*\phi_k^*\Omega_{ik}^{(\rho)}[\rho^*,m] + \phi_i\phi_k\Omega_{ik}^{(\rho)}[m^*,\rho^*])m_{kj}^{(F)} - U^2\sum_k \int_0^{t_i} dt_k\{\Omega_{ik}^{(\rho)}[\rho^*,\Pi] + \phi_i\phi_k^*(2\Omega_{ik}^{(\rho)}$$
$$\times[\rho,\rho^*] + \Omega_{ik}^{(\rho)}[m,m^*])\}m_{kj}^{(F)} + U^2\sum_k \int_0^{t_j} dt_k(\phi_i^*\phi_k\Omega_{ik}^{(F)}[m,\rho^*] + \phi_i^*\phi_k^*\Omega_{ik}^{(F)}[m,m] + \phi_i\phi_k^*\Omega_{ik}^{(F)}[\rho,m])\rho_{kj}^{(\rho)}$$
$$+ U^2\sum_k \int_0^{t_j} dt_k\{\Omega_{ik}^{(F)}[m,\Pi] + \phi_i\phi_k(2\Omega_{ik}^{(F)}[\rho,\rho^*] + \Omega_{ik}^{(F)}[m,m^*])\}\rho_{kj}^{(\rho)} + U^2\sum_k \int_0^{t_j} dt_k(\phi_i^*\phi_k\Omega_{ik}^{(F)}[\rho^*,\rho^*] + \phi_i^*\phi_k^*\Omega_{ik}^{(F)}[\rho^*,m]$$
$$+ \phi_i\phi_k\Omega_{ik}^{(F)}[m^*,\rho^*])m_{kj}^{(\rho)} + U^2\sum_k \int_0^{t_j} dt_k\{\Omega_{ik}^{(F)}[\rho^*,\Pi] + \phi_i\phi_k^*(2\Omega_{ik}^{(F)}[\rho,\rho^*] + \Omega_{ik}^{(F)}[m,m^*])\}m_{kj}^{(\rho)}, \tag{B13}$$

$$i\hbar\partial_{t_i} m_{ij}^{(\rho)} = -J[m_{i+1j}^{(\rho)}(t_i,t_j) + m_{i-1j}^{(\rho)}(t_i,t_j)] + 2U(|\phi_i|^2 + \rho_{ii}^{(F)})m_{ij}^{(\rho)} + U(m_{ii}^{(F)} + \phi_i^2)\rho_{ij}^{(\rho)} + U^2\sum_k \int_{t_j}^{t_i} dt_k(\phi_i^*\phi_k\Omega_{ik}^{(\rho)}[m,\rho^*] + \phi_i^*\phi_k^*\Omega_{ik}^{(\rho)}$$
$$\times[m,m] + \phi_i\phi_k^*\Omega_{ik}^{(\rho)}[\rho,m])\rho_{kj}^{(\rho)} + U^2\sum_k \int_{t_j}^{t_i} dt_k\{\Omega_{ik}^{(\rho)}[m,\Pi] + \phi_i\phi_k(\Omega_{ik}^{(\rho)}[\rho,\rho^*] + 2\Omega_{ik}^{(\rho)}[m,m^*])\}\rho_{kj}^{(\rho)}$$
$$+ U^2\sum_k \int_{t_j}^{t_i} dt_k(\phi_i^*\phi_k\Omega_{ik}^{(\rho)}[\rho^*,\rho^*] + \phi_i^*\phi_k^*\Omega_{ik}^{(\rho)}[\rho^*,m] + \phi_i\phi_k\Omega_{ik}^{(\rho)}[m^*,\rho^*])m_{kj}^{(\rho)} + U^2\sum_k \int_{t_j}^{t_i} dt_k\{\Omega_{ik}^{(\rho)}[\rho^*,\Pi] + \phi_i\phi_k^*(2\Omega_{ik}^{(\rho)}$$
$$\times[\rho,\rho^*] + \Omega_{ik}^{(\rho)}[m,m^*])\}m_{kj}^{(\rho)}, \tag{B14}$$

with

$$\Pi_{ij}^{(F,\rho)} = \Omega_{ij}^{(F,\rho)}[\rho,\rho^*] + \Omega_{ij}^{(F,\rho)}[m,m^*]. \tag{B15}$$

In the above equations we have simplified the notation replacing $\phi_k(t_k)$ by ϕ_k and $m_{kj}(t_k,t_j)$ by m_{kj}.

[1] M. Greiner, *et al.*, Nature (London) **415**, 39 (2002).
[2] S. Inouye *et al.*, Nature (London) **392**, 151 (1998).
[3] C. Regal *et al.*, Nature (London) **424**, 47 (2003).
[4] E. Donley *et al.*, Nature (London) **417**, 529 (2002).
[5] S. Peil, *et al.*, Phys. Rev. A **67**, 051603 (2003).
[6] A. M. Rey, P. B. Blakie, and C. W. Clark, Phys. Rev. A **67**, 053610 (2003).
[7] H. Shi and A. Griffin, Phys. Rep. **304**, 1 (1998); A. Griffin, Phys. Rev. B **53**, 9341 (1995).
[8] R. Walser *et al.*, Phys. Rev. A **59**, 3878 (1999); R. Walser, J. Cooper, and M. Holland, *ibid.* **63**, 013607 (2000); J. Wachter, R. Walser, J. Cooper, and M. Holland, *ibid.* **64**, 053612 (2001).
[9] C. W. Gardiner and P. Zoller, Phys. Rev. A **61**, 033601 (2000); C. W. Gardiner, J. R. Anglin, and T. I.A. Fudge, e-print cond-mat/0112129; C. W. Gardiner and M. J. Davis, e-print cond-mat/0308044.
[10] J. S. Schwinger, J. Math. Phys. **2**, 407 (1961); L. V. Keldysh, Zh. Eksp. Teor. Fiz. **47**, 1515 (1964) [Sov. Phys. JETP **20**, 1018 (1965)]; G. Zhou, Z. Su, B. Hao, and L. Yu, Phys. Rep. **118**, 1 (1985).
[11] J. Luttinger and J. Ward, Phys. Rev. **118**, 1417 (1960); C. de Dominicis and P. Martin, J. Math. Phys. **5**, 14 (1964); H. D. Dahmen and G. Jona Lasino, Nuovo Cimento A **52**, 807 (1967); J. M. Cornwall, R. Jackiw, and E. Tomboulis, Phys. Rev. D **10**, 2428 (1974).
[12] E. Calzetta and B. L. Hu, Phys. Rev. D **37**, 2878 (1988).
[13] E. Calzetta and B. L. Hu, in *Heat Kernel Techniques and Quantum Gravity*, edited by S. A. Fulling, Discourses in Mathematics and Its Applications Vol. 4 (A&M University Press, College Station, TX, 1995); Phys. Rev. D **61**, 025012 (2000).
[14] E. A. Calzetta, B. L. Hu, and S. A. Ramsey, Phys. Rev. D **61**, 125013 (2000).
[15] E. Calzetta and B. L. Hu, Phys. Rev. D **35**, 495 (1987).
[16] S. A. Ramsey and B. L. Hu, Phys. Rev. D **56**, 661 (1997).
[17] E. Calzetta and B. L. Hu, Phys. Rev. D **40**, 656 (1989).
[18] D. Bodeker, Nucl. Phys. B **559**, 502 (1999); **566**, 402 (2000); J. Blaizot and E. Iancu, Phys. Rep. **359**, 355 (2002).
[19] H. T. C. Stoof, in *Coherent Atomic Matter Waves*, Proceedings of the Les Houches Summer School Session 72, 1999, edited by R. Kaiser *et al.* (Springer-Verlag, Berlin, 2001).
[20] D. Boyanovsky, Ann. Phys. (N.Y.) **300**, 1 (2002).

[21] J. Rammer, *Quantum Transport Theory* (Perseus, Reading, MA, 1998).
[22] F. Cooper, S. Habib, Y. Kluger, E. Mottola, J. P. Paz, and P. R. Anderson, Phys. Rev. D **50**, 2848 (1994); Bogdan Mihaila, John F. Dawson, and F. Cooper, *ibid.* **56**, 5400 (1997); Bogdan Mihaila, John F. Dawson, and F. Cooper, *ibid.* **63**, 096003 (2001); Bogdan Mihaila *et al.*, *ibid.* **62**, 125015 (2000).
[23] G. Aarts *et al.*, e-print hep-ph/0201308; J. Berges, Nucl. Phys. A **699**, 847 (2002); J. Berges and J. Cox, Phys. Lett. B **517**, 369 (2001); G. Aarts and J. Berges, Phys. Rev. D **64**, 105010 (2001).
[24] F. Lombardo, F. D. Mazzitelli, and R. Rivers, e-print hep-ph/0204190.
[25] Ana M. Rey *et al.*, J. Phys. B **36**, 825 (2003); K. Burnett, M. Edwards, C. W. Clark, and M. Shotter, *ibid.* **35**, 1671 (2002).
[26] M. P. A. Fisher, P. B. Weichman, G. Grinstein, and D. S. Fisher, Phys. Rev. B **40**, 546 (1989); D. van Oosten, P. van der Straten, and H. T. C. Stoof, Phys. Rev. A **63**, 053601 (2001).
[27] A. Polkovnikov, S. Sachdev, and S. M. Girvin, Phys. Rev. A **66**, 053607 (2002).
[28] Markus Greiner, Olaf Mandel, Theodor W. Haensch, and Immanuel Bloch, e-print cond-mat/0207196.
[29] E. M. Wright, T. Wong, M. J. Collett, S. M. Tan, and D. F. Walls, Phys. Rev. A **56**, 591 (1997); A. J. Leggett and F. Sols, Found. Phys. **21**, 353 (1991); F. Sols, Physica B **194**, 1389 (1994); A. Smerzi and S. Raghavan, Phys. Rev. A **61**, 063601 (2000).
[30] S. A. Morgan, Ph.D. thesis, Oxford University, 1999 (unpublished); S. A. Morgan, J. Phys. B **57**, 3847 (2000); e-print cond-mat/0307246.
[31] D. A. W. Hutchinson *et al.*, J. Phys. B **57**, 3825 (2000).
[32] P. Hohenberg and P. Martin, Ann. Phys. (N.Y.) **34**, 291 (1965).
[33] S. Giorgini, Phys. Rev. A **57**, 2949 (1997); **61**, 063615 (2000).
[34] N. P. Proukakis and K. Burnett, J. Res. Natl. Inst. Stand. Technol. **101**, 457 (1996); N. P. Proukakis and K. Burnett, and H. T.C. Stoof, Phys. Rev. A **57**, 1230 (1998); T. Kohler and K. Burnett, *ibid.* **65**, 033601 (2002).
[35] S. T. Beliaev, Zh. Eksp. Teor. Fiz. **34**, 433 (1958) [Sov. Phys. JETP **7**, 299 (1958)].
[36] V. N. Popov, *Functional Integrals in Quantum Field Theory and Statistical Physics* (Reidel, Dordrecht, 1983).
[37] M. Bijlsma and H. T. C. Stoof, Phys. Rev. A **55**, 498 (1996); Jens O. Andersen, e-print cond-mat/0305138.
[38] Emil Lundh and Jorgen Rammer, Phys. Rev. A **66**, 033607 (2002).
[39] J. Wachter, R. Walser, J. Cooper, and M. Holland, e-print cond-mat/0212432.
[40] L. P. Kadanoff and G. Baym, *Quantum Statistical Mechanics: Green's Function Methods in Equilibrium and Nonequilibrium Problems* (Addison-Wesley, New York, 1962).
[41] B. L. Hu and D. Pavon, Phys. Lett. B **180**, 329 (1986); H. E. Kandrup, Phys. Rev. D **37**, 3505 (1988); **38**, 1773 (1988); S. Habib, Y. Kluger, E. Mottola, and J. P. Paz, Phys. Rev. Lett. **76**, 4660 (1996); Y. Kluger, E. Mottola, and J. M. Eisenberg, Phys. Rev. D **58**, 125015 (1998).
[42] We make a distinction between the meaning of the words "damping" and "dissipation," the former referring simply to the phenomenological decay of some function and the latter to theoretical meaning, e.g., in the Boltzmann sense.
[43] R. Balescu, *Equilibrium and Nonequilibrium Statistical Mechanics* (Wiley, New York, 1975).
[44] S. G. Bhongale, R. Walser, and M. J. Holland, Phys. Rev. A **66**, 043618 (2002).
[45] G. Baym, Phys. Rev. **127**, 1391 (1962); Baym B. Vanderheyden and G. Baym, J. Stat. Phys. **93**, 843 (1998); M. Bonitz, *Progress in Nonequilibrium Green's Functions* (World Scientific, Singapore, 2000).
[46] R. Rajaraman, *Solitons and Instantons* (Elsevier, Amsterdam, 1987).
[47] U. Al Khawaja, J. O. Andersen, N. P. Proukakis, and H. T. C. Stoof, Phys. Rev. A **66**, 013615 (2002).
[48] C. W. Gardiner, Phys. Rev. A **56**, 1414 (1997).
[49] The HFB approximation can be seen as a quadratic approximation of the Hamiltonian in which third and quadric terms are reduced to linear and quadratic forms by factorizing them in a self-consistent Gaussian approximation. Any quadratic Hamiltonian can be diagonalized exactly and this is achieved by transforming to a quassiparticle basic, $\{\hat{\alpha}_q\}$. The requirement of the transformation to be cononical means that it preserves communication relation and leads to bosonic quassiparticles.